AD-A172 694 THEORETICAL AND EXPERIMENTAL ANALYSIS OF MULTIDIRECTIONALLY-BRAIDED COMPO... (U) DAVID W TAYLOR NAVAL SHIP RESEARCH AND DEVELOPMENT CENTER ANN... 1/1

UNCLASSIFIED E T CAMPONESCHI ET AL. SEP 86 F/G 11/4 NL

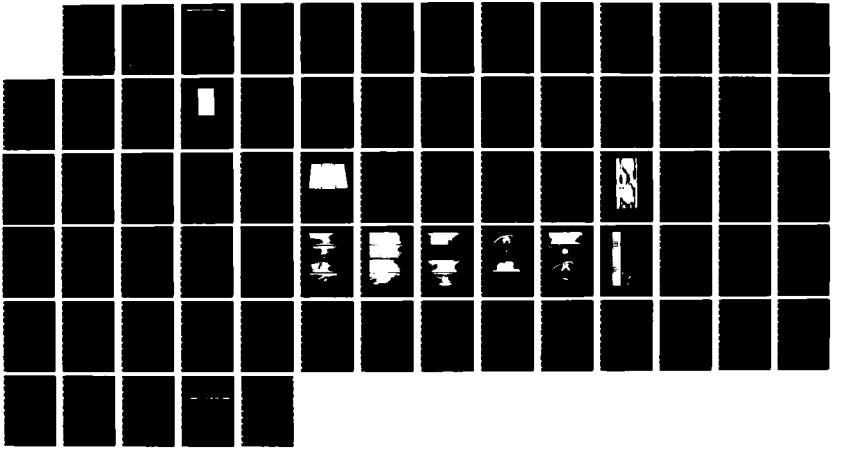

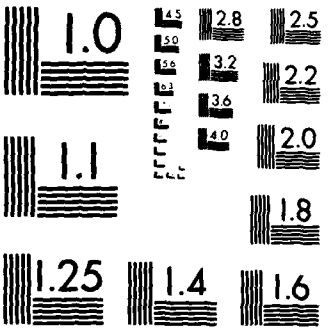

David W. Taylor Naval Ship Research and Development Center

Bethesda, MD 20084-5000

SME-86-75 September 1986

Ship Materials Engineering Department

Departmental Report

Theoretical and Experimental Analysis of Multidirectionally-Braided Composites

by

E.T. Camponeschi, Jr.

L.L. Wall

R.M. Crane

Approved for public release; distribution is unlimited.

MAJOR DTNSRDC TECHNICAL COMPONENTS

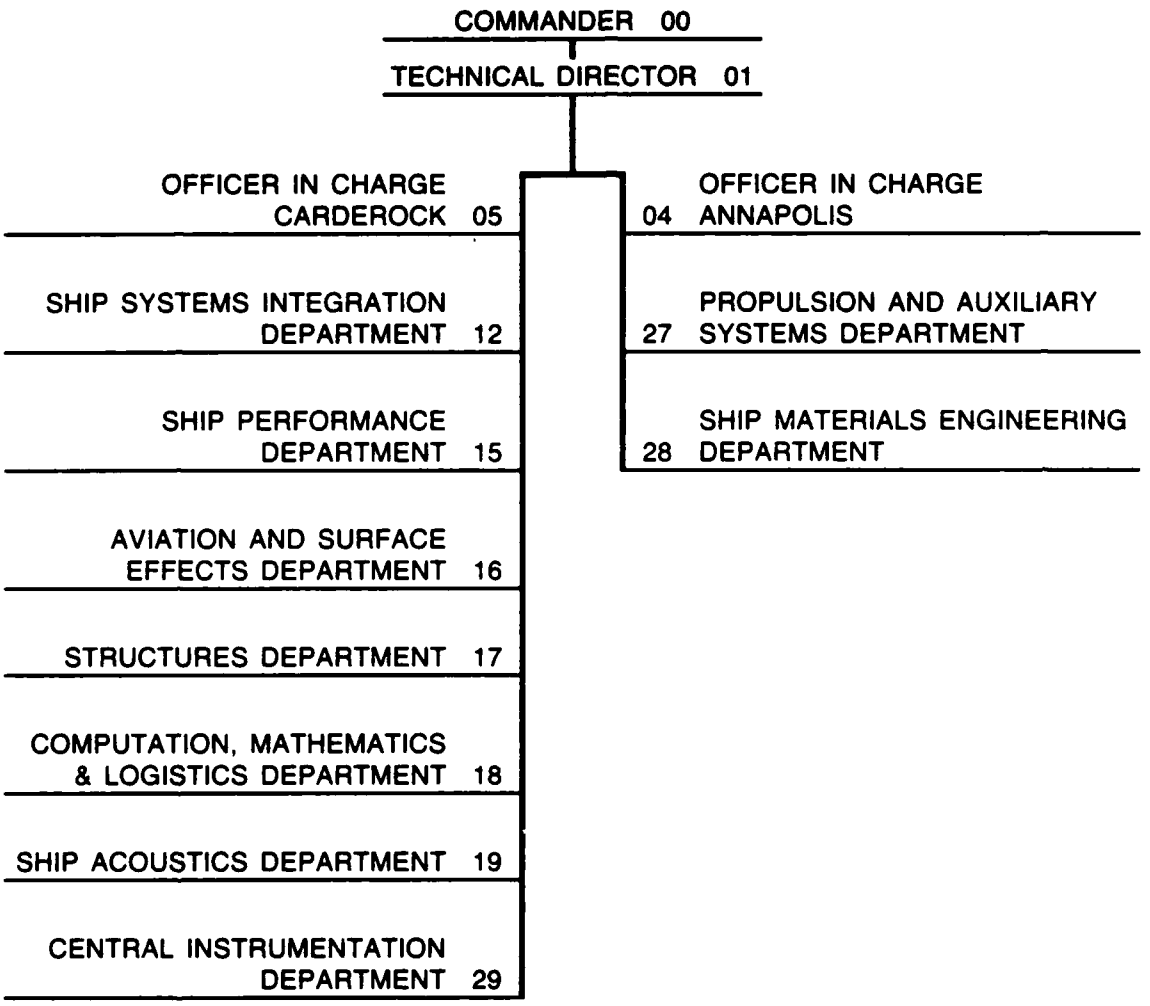

UNCLASSIFIED
SECURITY CLASSIFICATION OF THIS PAGE

AD-A172 694

REPORT DOCUMENTATION PAGE

1a. REPORT SECURITY CLASSIFICATION UNCLASSIFIED	1b. RESTRICTIVE MARKINGS
2a. SECURITY CLASSIFICATION AUTHORITY	3. DISTRIBUTION/AVAILABILITY OF REPORT Approved for Public Release; Distribution Unlimited.
2b. DECLASSIFICATION/DOWNGRADING SCHEDULE	
4. PERFORMING ORGANIZATION REPORT NUMBER(S) DTNSRDC/SME-86-75	5. MONITORING ORGANIZATION REPORT NUMBER(S)
6a. NAME OF PERFORMING ORGANIZATION David Taylor Naval Ship R&D Center 6b. OFFICE SYMBOL (If applicable) Code 2844	7a. NAME OF MONITORING ORGANIZATION
6c. ADDRESS (City, State, and ZIP Code) Bethesda, MD 20084-5000	7b. ADDRESS (City, State, and ZIP Code)
8a. NAME OF FUNDING/SPONSORING ORGANIZATION 8b. OFFICE SYMBOL (If applicable)	9. PROCUREMENT INSTRUMENT IDENTIFICATION NUMBER
8c. ADDRESS (City, State, and ZIP Code)	10. SOURCE OF FUNDING NUMBERS

PROGRAM ELEMENT NO.	PROJECT NO.	TASK NO.	WORK UNIT ACCESSION NO.
62766N	Z66300	RZ66300	1-2844-395

11. TITLE (Include Security Classification)
Theoretical and Experimental Analysis of Multidirectionally-Braided Composites

12. PERSONAL AUTHOR(S)
E. T. Camponeschi, Jr., L. L. Wall, and R. M. Crane

13a. TYPE OF REPORT	13b. TIME COVERED	14. DATE OF REPORT (Year, Month, Day)	15. PAGE COUNT
Departmental	FROM 10/83 TO 9/86	86 September	68

16. SUPPLEMENTARY NOTATION

17 COSATI CODES			18. SUBJECT TERMS (Continue on reverse if necessary and identify by block number)
FIELD	GROUP	SUB-GROUP	Multidirectionally Braided Composites Stiffness Model Damage Model Theoretical Modeling Impact Model Experimental Testing

19. ABSTRACT (Continue on reverse if necessary and identify by block number)

The ability of multidirectionally (X-D) braided composites to contain damage is one of the major advantages offered by this material. This report describes the development of analytical methods for determining the fiber geometry, stiffness, and impact damage response of X-D braided composites. The fiber geometry model is based on the braid parameters used in the construction of X-D braided composites. The stiffness model is based on this fiber geometry model and laminated plate theory. The impact damage model is based on the braided fiber geometry and the fracture toughness of the resin system used in the X-D composite.

This report also describe the results of experimental studies conducted to evaluate the results of the theoretical models.

20. DISTRIBUTION/AVAILABILITY OF ABSTRACT	21. ABSTRACT SECURITY CLASSIFICATION
☐ UNCLASSIFIED/UNLIMITED ☒ SAME AS RPT ☐ DTIC USERS	Unclassified

22a. NAME OF RESPONSIBLE INDIVIDUAL	22b. TELEPHONE (Include Area Code)	22c. OFFICE SYMBOL
E. T. Camponeschi	301-267-2165	Code 2844

DD FORM 1473, 84 MAR 83 APR edition may be used until exhausted
All other editions are obsolete

SECURITY CLASSIFICATION OF THIS PAGE

CONTENTS

FIGURES

FIGURES (Continued)

TABLES

TABLES (Continued)

ABBREVIATIONS AND SYMBOLS

avg	average
CMZ	column movement, z-direction
DCB	Double Cantilever Beam
E	modulus of elasticity
E_{INT}	intersection toughness
G	strain energy release rate
in-lb	inch-pound
$in\text{-}lb/in^2$	inch-pounds per square inch
INT	integer portion of
kV	kilovolts
lbf/in^2	pounds per square inch
mA	milliampere
mL	milliliter
NC	number of columns
NR	number of rows
PPL	plaits per length
REM	remainder of
RMY	row movement, y-direction
ν	Poisson's ratio

ABSTRACT

The ability of multidirectionally (X-D) braided composites to contain damage is one of the major advantages offered by this material. This report describes the development of analytical methods for determining the fiber geometry, stiffness, and impact damage response of X-D braided composites. The fiber geometry model is based on the braid parameters used in the construction of X-D braided composites. The stiffness model is based on this fiber geometry model and laminated plate theory. The impact damage model is based on the braided fiber geometry and the fracture toughness of the resin system used in the X-D composite.

This report also describes the results of experimental studies conducted to evaluate the results of the theoretical models.

ADMINISTRATIVE INFORMATION

This project was supported by the DTNSRDC Independent Exploratory Development Program, sponsored by the Space and Naval Warfare Systems Command, Director of Navy Laboratories, SPAWAR 05 and administered by the Research Coordinator, DTNSRDC, 012.3, under Program Element 62766N, Task Area RZ66300, and DTNSRDC Work Unit 1-2844-395.

INTRODUCTION

Fiber-reinforced composite materials have exhibited widespread success in numerous aerospace applications and consequently are under consideration as a material system for future naval applications. Multidirectionally (X-D) braided composite materials are of particular interest for certain applications due to their resistance to impact damage and ability to be braided to net-shape.

A description of the X-D braiding process referred to in this paper can be found in papers by Macander et al.[1] and Gauss and Alper[2]. In order to begin to utilize the advantages offered by X-D braided composites, a more complete understanding of the theoretical and experimental mechanical response of this system is required. Prior to conducting a theoretical mechanics analysis, it is necessary to understand the fiber geometry generated by the X-D braiding process. This paper describes the results of an effort to develop a model for the fiber geometry in braided composites as a function of the braiding parameters, and to develop a stiffness model based on this fiber geometry and laminated plate theory. This task was undertaken to complement an experimental investigation on X-D braided composites conducted at the David Taylor Naval Ship Research and Development Center by Macander et al.[3]. In performing that experimental task, the need for a model describing the fiber geometry in X-D braided composites became evident. The work described in this paper specifically addresses that need and further uses the fiber geometry information to develop an approximate stiffness model for X-D braided composites.

The output from the fiber geometry model is also used in conjunction with the concept of strain-energy release rate to develop an impact damage model for X-D braided composite panels.

Following the development of the fiber geometry, stiffness, and impact damage models, an experimental investigation was conducted to verify their accuracy. These verifications were performed by inspecting braids with visible tracer fibers to verify the fiber geometry model, by comparing experimental stiffness results to the theoretical stiffness model, and by comparing drop-ball impact test results to the results of the impact damage model.

THEORETICAL ANALYSIS

FIBER GEOMETRY MODEL

The most fundamental parameters that can be used to predict the fiber geometry of an X-D braided composite are: fiber tow size, number of rows in the loom, number of columns in the loom, and the braid pattern in which the loom bed carriers move. A schematic of a rectangular loom is shown in Fig. 1. The information needed to characterize a braided composite that can be derived from the above parameters includes: item dimensions, braid repeat, and most importantly, the fiber geometry. The item dimensions and braid repeat characteristics of a braided composite, however, will vary with longitudinal fiber compaction and resin impregnation procedures. Therefore, the basis of the present analysis will be to model braid fiber geometry as a function of the number of rows in the loom, the number of columns in the loom, the braid pattern, the final item dimensions, and the characteristic braid repeat length.

Figure 2 shows the geometry of a rigidized flat braided composite panel of rectangular cross-section. The X-Y and X-Z views of this panel include the projected image of a single continuous fiber tow contained within the panel. Figure 2 shows that the projected surface angles (θxy and θxz) of a braided composite can be determined if the panel width (W), the panel thickness (T), and the distance necessary for a tow to return to its original along-the-length position are known. The panel width and panel thickness are easily determined for a rigidized panel, while the determination of L_1 and L_2 is not immediately obvious. Based on a method for determining L_1 and L_2 for simple braids described by Brunnschweiler[4], L_1 and L_2 can be determined for X-D braided composites.

GIVEN:

FIBER TOW SIZE

- NUMBER OF ROWS (NR)
- NUMBER OF COLUMNS (NC)
- BRAID PATTERN (1 × 1, 3 × 1, ETC.)

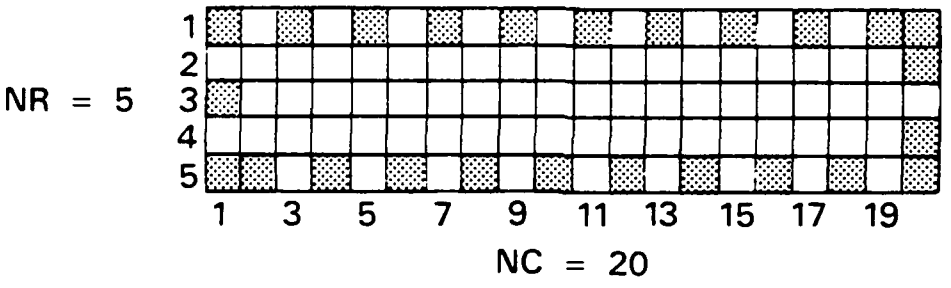

FIND:

- ITEM DIMENSIONS
- BRAID REPEAT
- FIBER GEOMETRY

Fig. 1. Fundamental braid parameters.

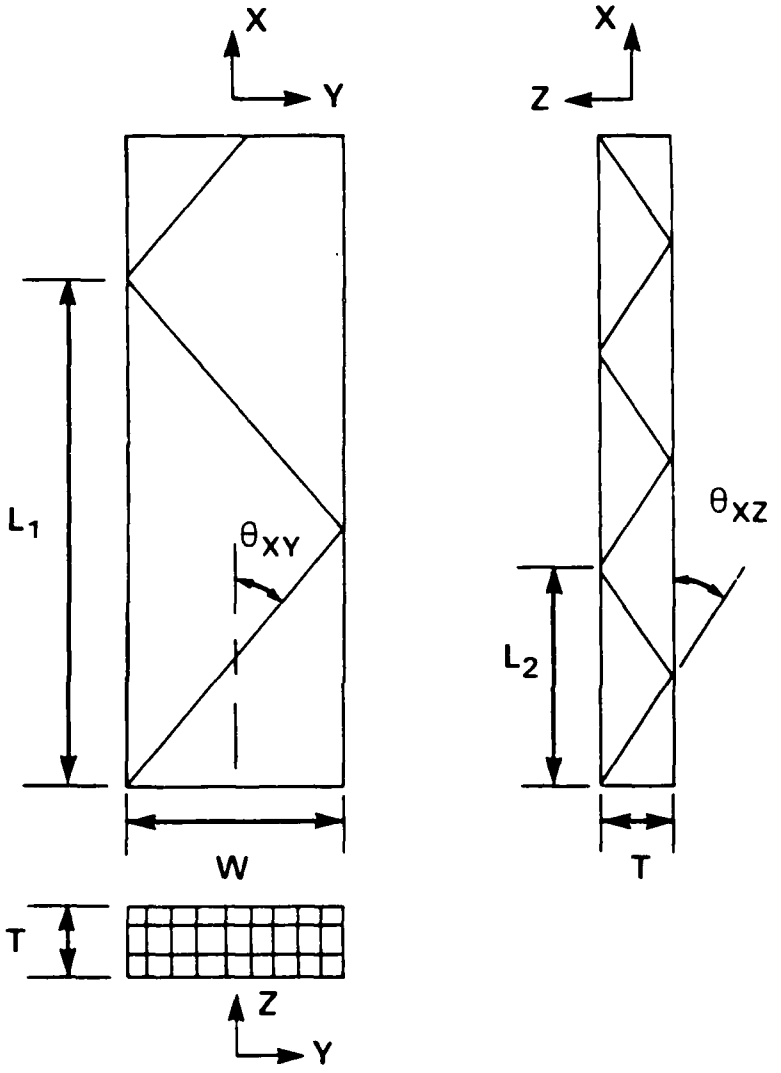

$$\text{TAN } \theta_{XY} = \frac{W}{L_1/2}$$

$$\text{TAN } \theta_{XZ} = \frac{T}{L_2/2}$$

Fig. 2. Braided panel geometry.

Brunnschweiler relates the number of fiber tows in a simple braid to the number of "plaits" longitudinally along the braid necessary for a single tow to return to its original along-the-length position. A "plait" can be recognized as the smallest visible repeating characteristic apparent on the surface of a braided panel.

Figure 3 shows the basis for determining the number of plaits required for a single tow to return to its original position, as shown in Fig. 2. The loom bed schematic shown in this figure is designed for a 3 x 1 rectangular braid in which NR=5, NC=25, and a total of 85 fiber tows make up the braid. The expressions for the number of plaits in L_1 and L_2 show how the longitudinal repeat is related to braid construction parameters. Specifically, the number of plaits in L_1 equals the number of horizontal row shifts necessary for a tow carrier to translate from one edge of the loom to the other. The number of plaits in L_2 equals the number of vertical column shifts necessary for a tow carrier to translate from one surface of the loom to the other. The left hand portion of the expression for L_1 accounts for the number of row movements in the repeating top to bottom translation, and the right hand portion of this expression accounts for the remainder of row movements after all of the repeating top to bottom translations are taken into account. In these expressions, INT stands for "integer portion of," REM for "remainder of." These expressions for L_1 and L_2 are for braids in which NC>NR and for which CMZ (column movement z-direction) equals 1. Expressions similar to these can be derived for NR>NC, NR=NC, or CMZ>1.

Following the determination of the number of plaits in L_1 and L_2, the distance spanned by this number of plaits must be determined. This distance is determined from the rigidized braid in question, as shown in Fig. 4. For

$$L_1: \left\{(NR-1)INT\left[\frac{(NC-1)/RMY}{(NR-2)}\right]\right\} + \left\{REM\left[\frac{(NC-1)/RMY}{(NR-2)}\right]\right\}$$

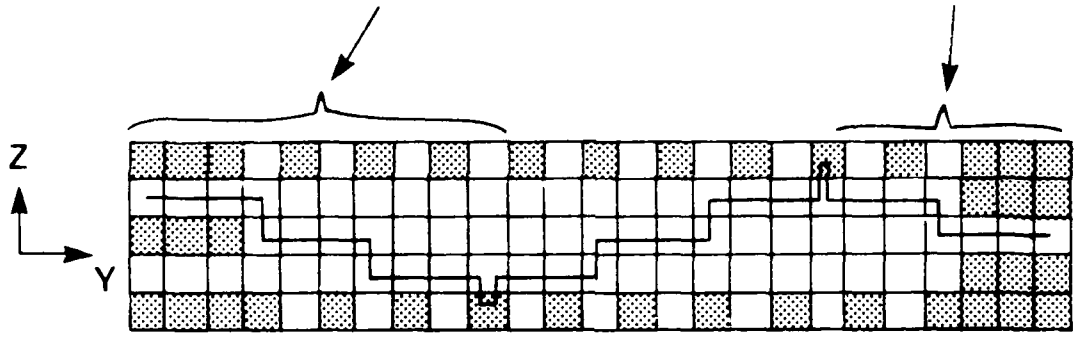

3 × 1 BRAID PATTERN
NR=5 NC=25

$$L_2: \frac{(NR-1)}{CMZ}$$

RMY = ROW MOVEMENT Y-DIRECTION $\boxed{3} \times 1$

CMZ = COLUMN MOVEMENT Z-DIRECTION $3 \times \boxed{1}$

Fig. 3. Number of plaits in L_1 and L_2.

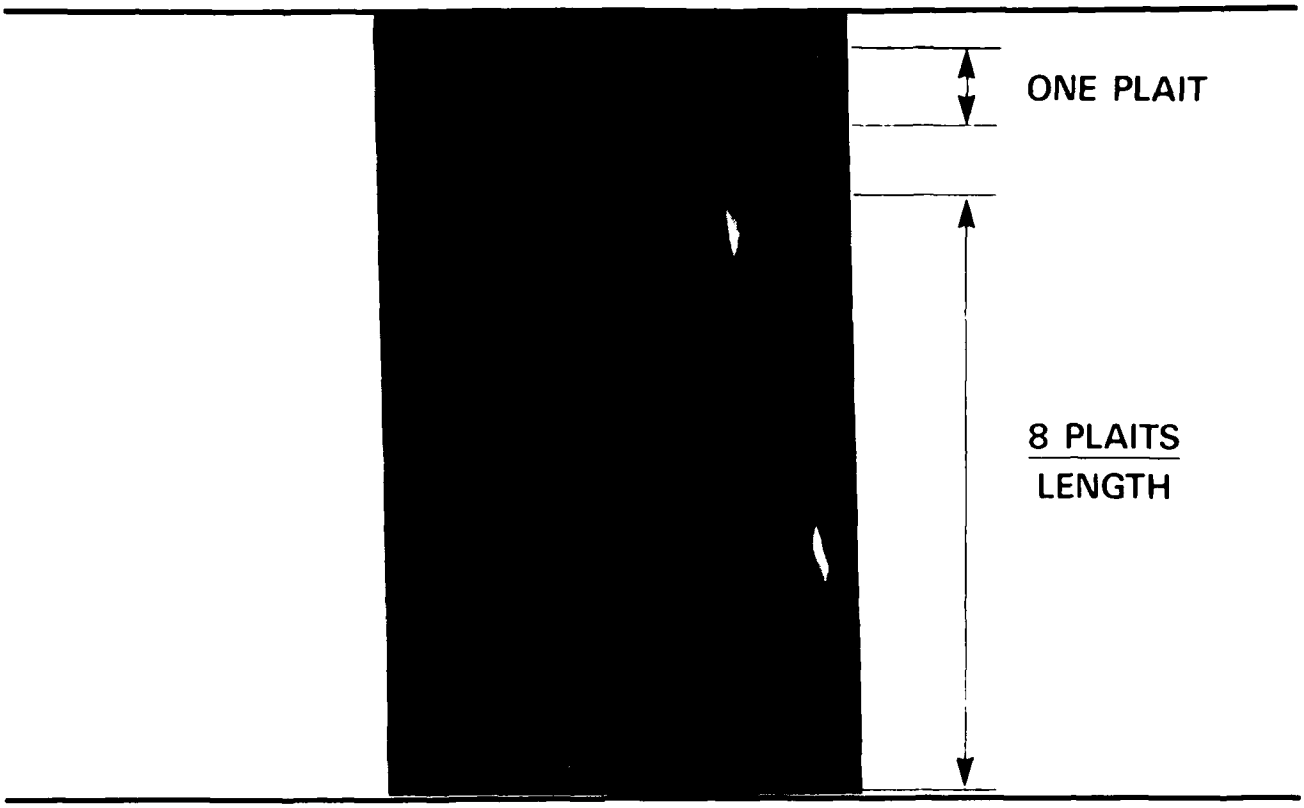

$$L_1 = \frac{\text{NUMBER OF PLAITS FOR LONGITUDINAL REPEAT}}{\text{PPL}}$$

$$L_2 = \frac{\text{NUMBER OF PLAITS FOR THICKNESS REPEAT}}{\text{PPL}}$$

Fig. 4. Definition of plaits per length, PPL.

any X number of plaits (8 plaits are used for the example shown), the distance these plaits span is measured on the braid under consideration and used to calculate the plaits per length (PPL) for this braid. The calculated value of PPL is then used for calculating the length of L_1 and L_2 by dividing the number of plaits for a longitudinal repeat (L_1) or thickness repeat (L_2) by the value of PPL.

From the preceeding discussion, it has been established that W, T, and PPL are determined from the rigidized braid under consideration, and NC, NR, RMY, and CMZ are given as braid construction parameters. Combining the relationships shown in Figs. 2, 3, and 4, it is now possible to establish the expressions for TAN θxy and TAN θxz, as shown in Fig. 5. These expressions then become the basis for any analytical characterization of braided composite materials. Although θxy and θxz are only the projected angles of a fiber in a braided composite, these two quantities are sufficient to describe the three-dimensional orientation of the fiber they represent.

Although the surface projection angles θxy and θxz are sufficient to describe the fiber geometry in an X-D braided composite, there are instances in which it is more convenient to express this fiber geometry in terms of the direction angles (α, β, γ) of a Cartesian coordinate system. If cos α, cos β, and cos γ are the direction cosines of vector A with respect to the x, y, and z axis, then these direction cosines can be expressed in terms of θxy and θxz only. This relationship between the projected angles (θxy and θxz) and a vector in three space (vector A) is shown in Fig. 6. The direction angles α, β, and γ will be instrumental in describing the subsequent stiffness analysis for X-D braids.

THEREFORE SINCE:

$$\text{TAN } \theta_{XY} = \frac{2W}{L_1} \qquad \text{TAN } \theta_{XZ} = \frac{2T}{L_2}$$

$$L_1 = \left\{ \text{INT} \left[\frac{(NC-1)/RMY}{(NR-2)} \right] + \frac{(NC-1)}{RMY} \right\} /PPL$$

$$L_2 = \left\{ \frac{(NR-1)}{CMZ} \right\} /PPL$$

THEN:

$$\text{TAN } \theta_{XY} = \frac{2\,(W)(PPL)}{\left\{ \text{INT} \left[\frac{(NC-1)/RMY}{(NR-2)} \right] + \frac{(NC-1)}{RMY} \right\}}$$

$$\text{TAN } \theta_{XZ} = \frac{2\,(T)(PPL)}{(NR-1)/CMZ}$$

Fig. 5. Derivation of theta XY and theta XZ.

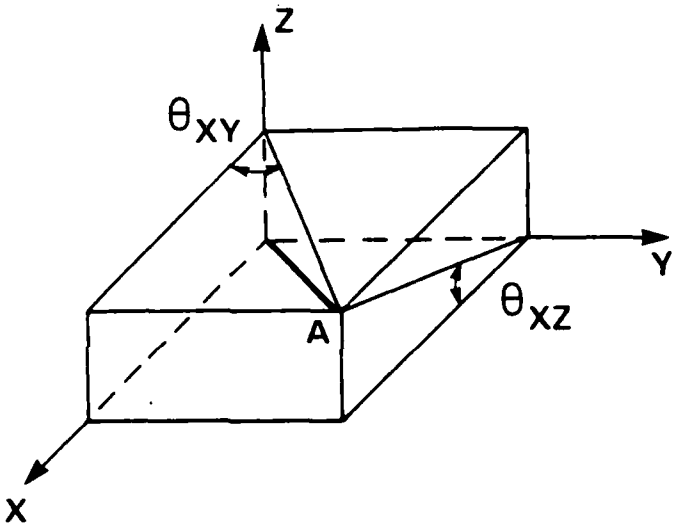

IF VECTOR IS DEFINED AS

$$[(X_1)i, (X_1 \text{ TAN } \theta_{XY})j, (X_1 \text{ TAN } \theta_{XZ})k]$$

LET COSα, COSβ, COSγ BE THE DIRECTION COSINES OF VECTOR A, THEN

$$\text{COS}\alpha = \frac{1}{\sqrt{1 + \text{TAN}^2\,\theta_{XY} + \text{TAN}^2\,\theta_{XZ}}}$$

$$\text{COS}\beta = \frac{\text{TAN}\,\theta_{XY}}{\sqrt{1 + \text{TAN}^2\,\theta_{XY} + \text{TAN}^2\,\theta_{XZ}}}$$

$$\text{COS}\gamma = \frac{\text{TAN}\,\theta_{XZ}}{\sqrt{1 + \text{TAN}^2\,\theta_{XY} + \text{TAN}^2\,\theta_{XZ}}}$$

Fig. 6. Definition of direction angles alpha, beta, and gamma.

STIFFNESS MODEL

An exploded view of the fiber geometry that makes up a braided composite is shown in Fig. 7. Both schematics in Fig. 7 are for a length (X-direction) of one plait. The upper schematic shows the actual fiber configuration that results from simple braider motions (1x1, 3x1, 2x1, etc.). The lower schematic shows the four fiber directions that account for the fiber geometry in a braided composite and is the most widely used representation of a braided structure. Unidirectional fill fibers may also be part of this structure and would follow the X, Y, or Z axis shown in Fig. 7. For the purposes of the present analysis, the effect of fiber undulation at the intersection points is not considered and consequently the fiber directions θxy, θxz, α, β, and γ are average fiber directions.

Now that the fiber geometry in an X-D braided composite is understood, a method for approximating Exx, Eyy, and Ezz in terms of this fiber geometry will be discussed. Figure 8 shows two schematics which include the four fiber directions that represent all of the fiber paths in an X-D braided composite with no longitudinal, transverse, or through-thickness fill fibers. These two schematics are the result of considering two diagonal sections of the unit cell shown in Fig. 7. It can be seen from Fig. 8 that by taking the correct diagonal slice of this unit, the four fiber directions are rotated $\alpha°$ from the longitudinal axis of the unit cell. Therefore, a calculation of Exx for a $(\pm\alpha)s$ laminate would result in a value of Exx that approximates the longitudinal modulus of the braided composite. To determine the effect of longitudinal fill fibers inserted into a braided panel, a $[(\pm\alpha)_n\ 0_m]_s$ laminate with the appropriate percentage of 0° plies can be analyzed.

SIMPLE BRAID FIBER GEOMETRY

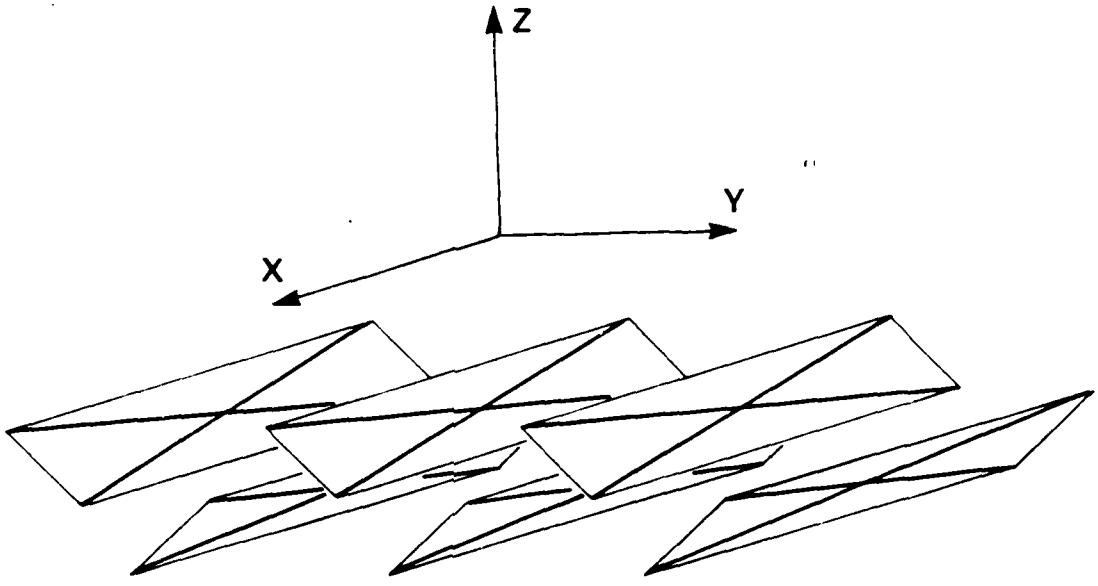

BRAID GEOMETRY REPRESENTATION

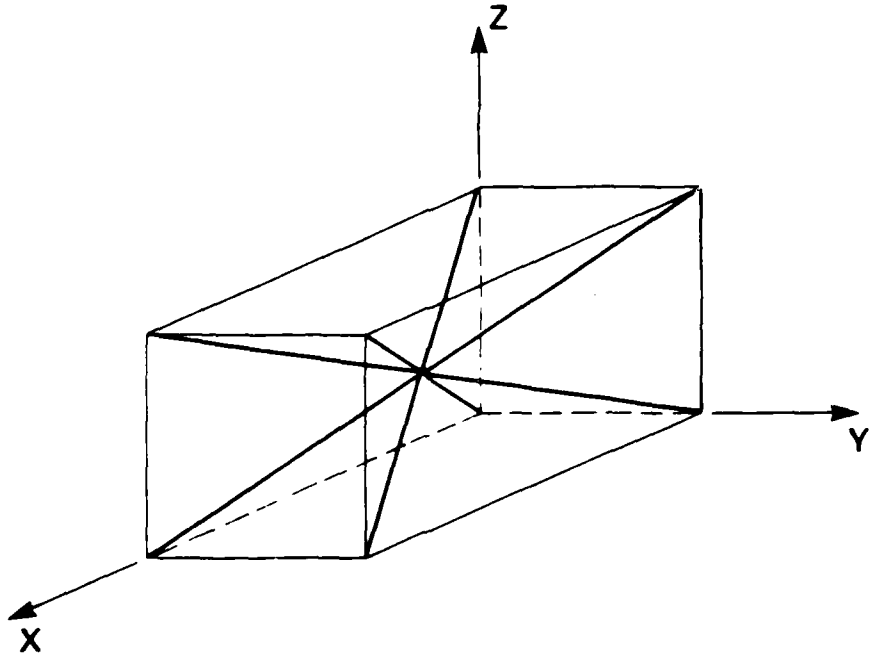

Fig. 7. Braided fiber structure.

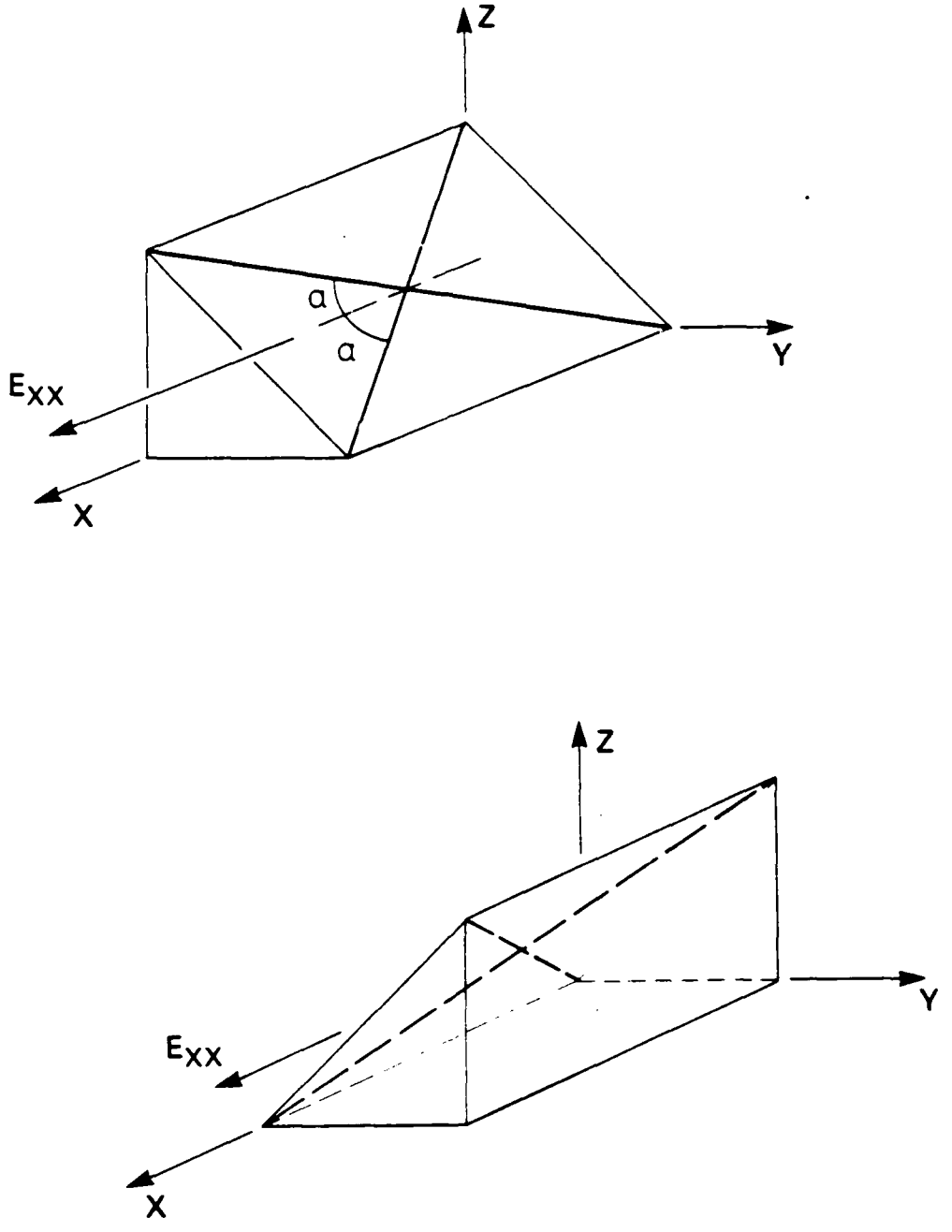

Fig. 8. The use of alpha for determining longitudinal modulus, E_{xx}.

The calculation of the transverse (Eyy) and through-thickness (Ezz) moduli for braided composites requires a diagonal sectioning procedure similar to the one performed to determine Exx. Figure 9 shows the diagonal slices required to determine Eyy and Ezz and illustrates the significance of β and γ in performing these moduli calculations. The utility of the described fiber geometry/stiffness model described here can now be recognized. Determining the fiber geometry of a braided composite in terms of the parameters described in Figs. 4 and 5 results in direction angles α, β, and γ, and these angles can be used directly in laminated plate theory for determination of the three principal geometric moduli of a braided composite panel.

The effect of longitudinal fill fibers on Eyy can be modeled with a $[(\pm\beta)n, 90m]_s$ laminate analogy, and the effect of transverse fill fibers on Eyy can be modeled with a $[(\pm\beta)_n, 0_m]_s$ laminate analogy with the appropriate ratio of m:n.

IMPACT DAMAGE MODEL

The impact damage model developed in this program was designed to account for the ability of braided composites to resist delamination. The creation of damage in composite materials due to an impact event is a complex phenonenom comprising damage that includes matrix cracking, fiber-matrix debonding, delamination, and fiber breakage. Consequently, a comprehensive theoretical model describing the overall impact of composites is not likely to be developed. Advancements have been made in the development of experimental techniques to characterize the delamination resistance of laminates, however, and these techniques show promise in accounting for improvements in delamination resistance attributed to tougher resin systems. These experimental techniques

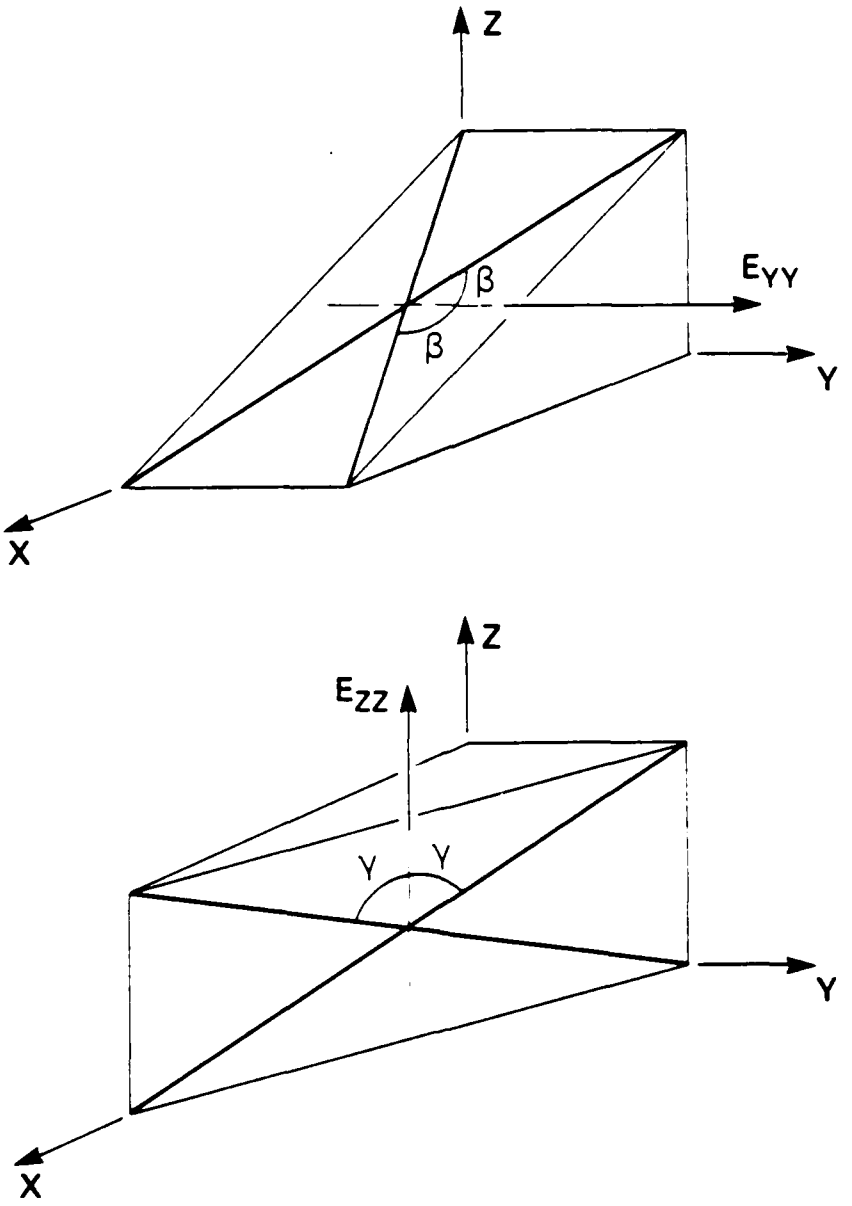

Fig. 9. The use of beta and gamma for determining E_{yy} and E_{zz}.

include Double Cantiliver Beam (DCB) tests discussed by Wilkins et al.[5], Free-Edge Delamination tests discussed by O'brien[6], and End Notched Flexure tests discussed by Gillespie and Carlsson.[7] These experimental techniques are not applicable to braided composite materials since the characterization of delamination is based upon fracture mechanics principles and assumptions (i.e. strain energy release rate and self-similar crack propagation). The fiber structure in braided composites that make them delamination resistant prohibits the use of fracture mechanics principles due to local inhomogeneity caused by fiber intersection locations.

Since delamination formation is a predominant feature of impact damage in composites, experimental programs have been conducted to correlate the extent of delamination to mode II strain energy release rate, G_{II}, Masters.[8] Since G_{II} is a measure of the energy necessary to create delamination, and damage is strongly proportional to the kinetic energy an impact specimen is subjected to, then impact damage should be related to kinetic impact energy as a function of G_{II}. This hypothesis is the basic assumption underlying the proposed damage model. This hypothesis implies that delamination type impact damage (units of area) is proportional to the impact energy imparted to a specimen divided by the energy necessary to create delaminations.

$$\text{Damage} = \frac{\text{Impact Energy}}{\text{Energy to Create Delaminations}} . \qquad (1)$$

G_{II}, however, is only a measure of delamination resistance for laminated composites, therefore the contribution to system toughness by the fiber intersections in a braided composite must be added to G_{II} in the denominator of Eq. 1.

$$\text{Damage} = \frac{\text{Impact Energy}}{\text{Matrix Toughness} \quad \text{Intersection Toughness}} \tag{2}$$

or

$$D(\text{in}^2) = \frac{W\ (\text{in-lb})}{G_{II}\left(\frac{\text{in-lb}}{\text{in}^2}\right) + N\ E_{INT}\left(\frac{\text{in-lb}}{\text{in}^2}\right)}, \tag{3}$$

where

D = damage area

W = impact energy

G_{II} = mode II interlaminar fracture toughness

N = number of intersections

E_{INT} = fiber intersection toughness

Values of G_{II} for currently available matrix systems have been reported; however, values for E_{INT} are unknown. For the purposes of this investigation, E_{INT} will be experimentally determined for various impact energies and two fiber geometries. These values of E_{INT} will then be used to determine values of damage area for any given impact energy.

The value of N in Eq. 3 is dependent on the damage area present in the damaged specimen, and the relationship between D and N is dependent upon the shape of the damage present in the specimen. The geometric relationship between damage shape and fiber intersection pattern is shown in Fig. 10 for circular and rectangular damage shapes. The expression relating N and D for rectangular damage is:

$$N = \text{INT}\ [DL \times PPL + 1] \times \text{INT}\ \left[\frac{DW \times (NC - RMY - 1)}{2W} +\right]$$

The value of N for circular damage is found by performing the following summation:

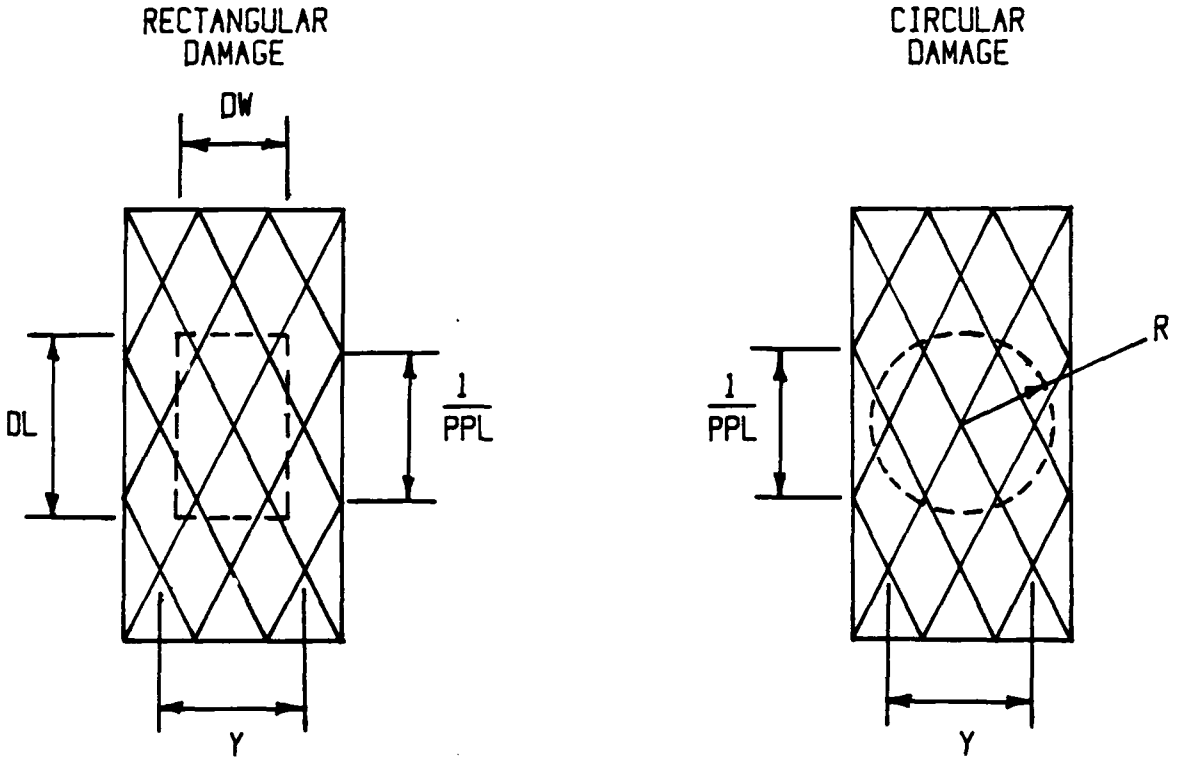

PPL = PLAITS PER LENGTH

Y = TRANSVERSE DISTANCE BETWEEN INTERSECTIONS

DL = DAMAGE LENGTH

DW = DAMAGE WIDTH

R = DAMAGE RADIUS

Fig. 10. Geometric relationship between fiber intersections and damage area.

N = 0

Y = 2 x W/(NC - RMY - 1)

D = Y/2

IF D > R, END

N = INT (2 x PPL x SQR (R^2 - D^2) + 1) + N

A listing of the computer code developed to run Eq. 3 for circular and rectangular impact damage is included in Figs. A.1 and A.2.

EXPERIMENTAL PROGRAM

SPECIMEN DESCRIPTION

Three braided specimen types and two laminated specimen types were evaluated in this study. Of the three braided specimen types, two were delivered as unimpregnated scarfs, and one was delivered as fully impregnated and rigidized specimens.

The impregnated specimen set comprised specimens manufactured by Milliken for a Virginia Polytechnic Institute braided composite characterization program, conducted by Stinchcomb et al.[9] Specimens 41 through 50 from the VPI program were sent to DTNSRDC for fiber geometry evaluation and stiffness testing. These test specimens were nominally 1 inch by 8 inches by 0.125 inches thick, and braided with a 1x1 construction in a 7x16 carrier rectangular loom. These specimens were AS-4, 12,000 filament graphite fiber and 3501 epoxy matrix.

Two multidirectionally-braided graphite scarves were purchased from Atlantic Research Corp. Both scarves were made using T-300 graphite fibers with 12,000 filaments per tow. The scarves were braided to finished dimensions of 2 inches wide, .10 inch thick, and a total length of 140 inches

each. Braid specifications were five rows and thirty-two columns using 1x1 braid construction. The scarves were combed to provide a fiber volume fraction of fifty-five to sixty-five percent. Additionally, one of the scarves was braided with twenty percent transverse fiber tows (12000 filament tows) inserted one per plait at the midplane of the scarf. The two braids were then cut into eight inch long pieces, which were impregnated with Narmco's 5208, 350 degree F. cure, epoxy resin using the impregnation technique developed at the David Taylor Naval Ship Research and Development Center by Crane and Macander.[10] Ten specimens from the 1x1 braid and eleven specimens from the 1x1 transverse filled braid (1x1T) were fabricated in this manner. A white, x-ray opaque tracer fiber was braided along with one fiber tow in the 1x1 scarf. This tracer was used to verify the calculation of the L_1 and L_2 as listed in Fig. 5.

Ten $[(\pm 20)_4]_s$ and twelve $[(\pm 30)_4 90_2]_s$ specimens were cut from laminates which were fabricated using T300/5208 prepreg. These specimens were autoclave cured according to manufacturer's specifications and specimen dimensions are given in Table 1.

Table 1. Average dimensions of test specimens.

Specimen Type	Avg. Width (in.)	Avg. Thick. (in.)	Nom. Length (in.)
1x1	2.0034	.0731	8
1x1T	2.0055	.1156	8
$[(\pm 20)_4]_s$	1.9997	.0807	8
$[(\pm 30)_4 90_2]_s$	1.9744	.1018	8

The fiber orientations for the laminated specimens were designed such that the $[(+-20)_4]_s$ laminates had in-plane properties comparable to the 1x1 braids, and the $[(+-30)_4 90_2]_s$ laminates had properties comparable to the 1x1T braids.

TENSION TESTING

In order to assess the damage tolerance of multidirectional (X-D) fiber reinforced composite materials, stiffness tests were performed on the four specimen groups before and after they were subjected to impact loading. The specimens were pulled to a predetermined strain level, located below the strain level expected to produce initial delamination, as documented by O'brien.[6] The 1x1 braids and the $[(+-20)_4]s$ laminates were tested to a level of .25 percent strain, while the 1x1T braids and the $[(+-30)_4 90_2]_s$ laminates were tested to a level of .1 percent strain.

A universal testing machine, fitted with 2-inch wide mechanical grips, was used to apply static loads to the specimens at a constant crosshead rate of .05 inches/minute. A 2-inch gage length extensometer was used to measure the strain level, which was plotted versus load on an X-Y recorder.

IMPACT TESTING

After performing the initial stiffness tests on all of the specimens, five specimens from each group were subjected to nominal impact energies of 24, 48, 72, 96 and 120 inch-pounds. The impact tests were performed using a drop ball impact machine. Stainless steel balls were used as indentors and varied in diameter from 1.75 inches to 2.125 inches. The drop heights were also adjusted to provide the desired impact energy. Rebound heights of the balls were recorded for each impact, in order to estimate the amount of energy absorbed by the specimens. Test results are shown in Table 2.

Table 2. Drop-Ball Impact Data.

Specimen	Ball Diameter (in.)	Weight (lb)	Drop Height (in.)	Impact Energy (in-lbs)	Rebound Height (in.)
20-1	1.75	.776	30.75	23.86	17
20-6	2.0	1.18	40.75	48.09	21
20-3	2.0	1.18	61.0	71.98	15
20-4	2.125	1.41	68.06	95.96	18
20-5	2.125	1.41	85.13	120.0	17
3090-1	1.75	.776	30.75	23.86	17
3090-2	2.0	1.18	40.75	48.09	16
3090-3	2.0	1.18	61.0	71.98	23
3090-4	2.125	1.41	68.06	95.96	24
3090-5	2.125	1.41	85.13	120.0	19
XD-6	1.75	.776	30.75	23.86	19
XD-1	2.0	1.18	40.75	48.09	25
XD-2	2.0	1.18	61.0	71.98	25
XD-4	2.125	1.41	68.06	95.96	20
XD-5	2.125	1.41	85.13	120.0	17
XD5T	1.75	.776	30.75	23.86	20
XD6T	2.0	1.18	40.75	48.09	24.5
XD7T	2.0	1.18	61.0	71.98	31
XD8T	2.125	1.41	68.06	95.96	31
XD9T	2.125	1.41	85.13	120.0	34

The specimens were clamped 5 inches along there length, from their edges, as shown in Fig. 11. After aligning the clamping fixture under the crosshead so the ball would impact the center of the specimen, it was bolted to the base plate of the impact machine. The underside of the specimen was unsupported outside the clamped area and supported by a steel plate 1.5 inches from each end of the specimen.

Residual stiffness tests were then performed on the impacted specimens.

X-RAY RADIOGRAPHY AND SECTIONING

X-ray radiography and sectioning techniques were used to develop three dimensional damage maps for the specimens subjected to impact damage. Dye

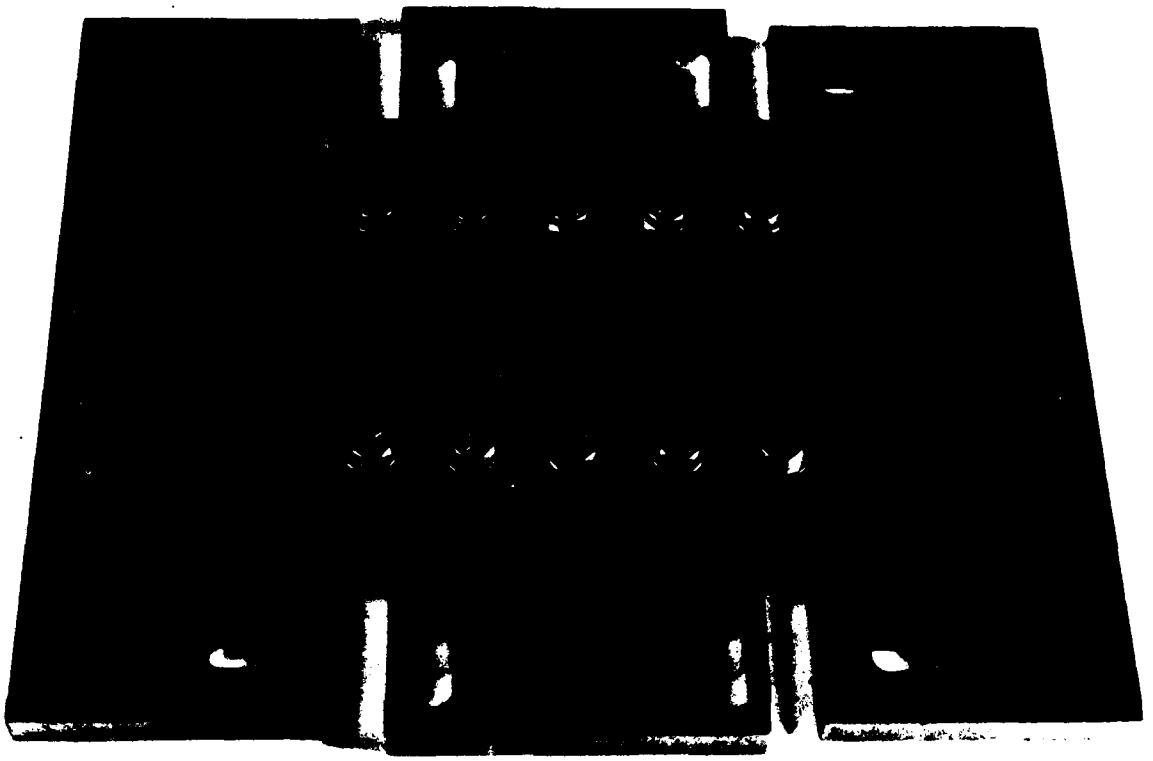

Fig. 11. Drop-ball impact test clamping fixture.

penetrant enhanced x-ray radiography was used to nondestructively inspect and record the extent of impact damage imparted to each specimen. A zinc iodide solution as described by Rummel[11] (60 grams ZnI_2, 10 ml. H_2O, 10 ml. Isopropyl Alcohol, 10 ml. Photo Flo 600) was used as the dye penetrant for these specimens. All x-ray exposures were 5.5 minutes at 40kV and 3mA with a source-to-film distance of 48 inches. A Torrex 120D x-ray cabinent and Kodak DR-S Industrex R film were used for all exposures. A stereo pair of x-rays were taken for each impacted specimen to assist in damage assessment. X-ray stereo pairs were exposed at 90° to the incident beam and 84° to the incident beam.

Following the non-destructive inspection of the impacted samples, each was sectioned, ground, polished, and photographed to further examine its damage state.

RESULTS AND DISCUSSION

FIBER GEOMETRY

The fiber geometry characteristic for each of the three braided systems investigated are listed in Tables A1, A2, and A3 in Appendix A. Theta XY and theta XZ are surface and edge projection angles as shown in Fig. 2, while alpha, beta, and gamma are the direction angles for each specimen as shown in Fig. 6. A summary of the fiber geometry for each of the three braid types is given in Table 3.

Table 3. Fiber geometry summary.

Specimen Type	PPL	θ_{xy} (°)	θ_{xz} (°)	α (°)	β (°)	γ (°)
1x1 (ARC)	3.50	18.9	7.28	20.0	71.3	83.1
1x1T (ARC)	4.92	25.6	15.9	29.1	65.3	75.7
1x1 (Milliken)	2.01	12.6	4.67	13.4	77.5	85.4

STIFFNESS

Based on the results of the fiber geometry model, theoretical values of E_{xx}, E_{yy}, and E_{zz} for each braided specimen type were calculated. These values are listed in Tables 4, 5, and 6.

Table 4. Theoretical stiffness for 1x1 T300/5208 braided panels.

Specimen	E_{xx} (10^6 psi)	E_{xy} (10^6 psi)	E_{zz} (10^6 psi)
XD1	15.1	1.65	1.59
XD2	13.9	1.66	1.59
XD3	15.9	1.64	1.59
XD4	13.4	1.67	1.59
XD5	15.0	1.65	1.59
XD6	13.3	1.68	1.59
XD7	11.6	1.71	1.59
XD8	15.5	1.64	1.59
XD9	13.4	1.67	1.59
XD10	13.7	1.67	1.59
XD12	15.0	1.65	1.59
Avg.	14.16	1.66	1.59

Table 5. Theoretical stiffness for 1x1 AS4/3501-6 braided panels.

Specimen	E_{xx} (10^6 psi)	E_{yy} (10^6 psi)	E_{zz} (10^6 psi)
41	17.2	1.62	1.58
42	16.9	1.62	1.59
43	16.9	1.62	1.59
44	16.7	1.63	1.59
45	17.4	1.62	1.58
46	17.4	1.62	1.58
47	17.5	1.62	1.58
48	17.5	1.62	1.58
49	16.8	1.63	1.59
50	17.5	1.62	1.58
Avg.	17.18	1.62	1.58

Table 6. Theoretical stiffness for 1x1T T300/5208 braided panels.

Specimen	E_{xx} (10^6 psi)	E_{yy} (10^6 psi)	E_{zz} (10^6 psi)
XD0T	8.0	5.70	1.65
XD1T	13.1	5.59	1.59
XD2T	9.36	5.68	1.62
XD3T	9.18	5.68	1.62
XD4T	8.77	5.69	1.63
XD5T	8.77	5.69	1.63
XD6T	9.71	5.66	1.62
XD7T	8.66	5.68	1.64
XD8T	10.7	5.63	1.62
XD9T	9.20	5.66	1.63
Avg.	9.55	5.66	1.65

In addition to the fiber geometry information, the following lamina data was used to generate these stiffnesses:

T300/5208	AS4/3501-6
$E_{11} = 21.3 \times 10^6$ psi	$E_{11} = 20.7 \times 10^6$ psi
$E_{22} = 1.58 \times 10^6$ psi	$E_{22} = 1.4 \times 10^6$ psi
$G_{12} = 0.9 \times 10^6$ psi	$G_{12} = 0.8 \times 10^6$ psi
$\nu_{12} = 0.28$	$\nu_{12} = 0.3$

Review of the average values for Exx and Eyy in Tables 4 and 5 indicate the highly orthotropic nature of 1x1 braids. The transverse (Eyy) modulus for both the T300 and AS4 fiber based systems is only slightly greater than Ezz of the unidirectional system. The effect of unidirectional transverse fill fibers can be seen in Table 6. For the 1x1 specimens evaluated here, a transverse fiber tow at the center of each plait and located along the neutral axis reduces Exx from 14.16×10^6 psi to 9.55×10^6 psi and increases Eyy from 1.66×10^6 psi to 5.66×10^6 psi. This braid construction does provide a braided panel with nearly quasi-isotropic properties. One drawback to this type of construction results from the extreme local fiber undulation the longitudinal braided fibers must undergo to pass over and under the transverse fill fibers. This extreme undulation caused resin-rich pockets or voids along the panels neutral axis resulting in lower than desired fiber volume fractions (average of 58.94%) and higher than desired void contents (average of 1.97%). Figure 12 shows a longitudinal section of a 1x1T specimen containing voids and resin-rich areas around the transverse fiber tows. Corrections to the molding procedure for transverse filled braids may provide better physical properties, however the transverse filled specimens fabricated for this evaluation were 0.009 inches thicker than the designed cure thickness. Although spacer material may be added to the mold cavity to reduce the speci-

Fig. 12. Photomicrograph of a longitudinal section of a 1 x 1T specimen.

men thickness, this fabrication experience suggests further compaction of the 1x1T specimens will be difficult.

Tables A4, A5, and A6 show a comparison of the theoretical and experimental values for Exx for the 1x1 and 1x1T braids. The bar graphs in Fig. 13 compare the theoretical and average experimental values for all of the specimen types tested. These graphs show that the experimental values were consistently lower than the corresponding theoretical prediction. Input data for the $[(+-20)_4]_s$ and $[(+-30)_4 90_2]_s$ laminates were the same as for the T300/5208 braids, and the predicted Exx was greater than the experimental values for these laminates also. Unidirectional laminate tests can be run to generate lamina properties that will account for processing and mechanical test variables specific to this test program. Corrections in lamina properties to adjust the experimental laminate stiffness will also adjust the theoretical braid stiffnesses to more accurately represent the experimental data.

Figures 14, 15, and 16 show plots containing each experimental data point generated to verify the X-D stiffness model. The experimental points on these graphs indicate the fiber geometry model can account for small changes in fiber geometry, which were evident in the experimental testing. The dashed line in Fig. 13, 14, and 15 is linear regression for the experimental data and closely parallels the slope of the theoretical stiffness plot.

IMPACT DAMAGE

Experimental drop-ball impact response was determined through stiffness measurements, X-ray radiography and cross-sectioning inspections. Figures 17 and 18 show the results of stiffness measurements taken after impact damage had been imparted to both the braided and laminated specimens. The stiffness

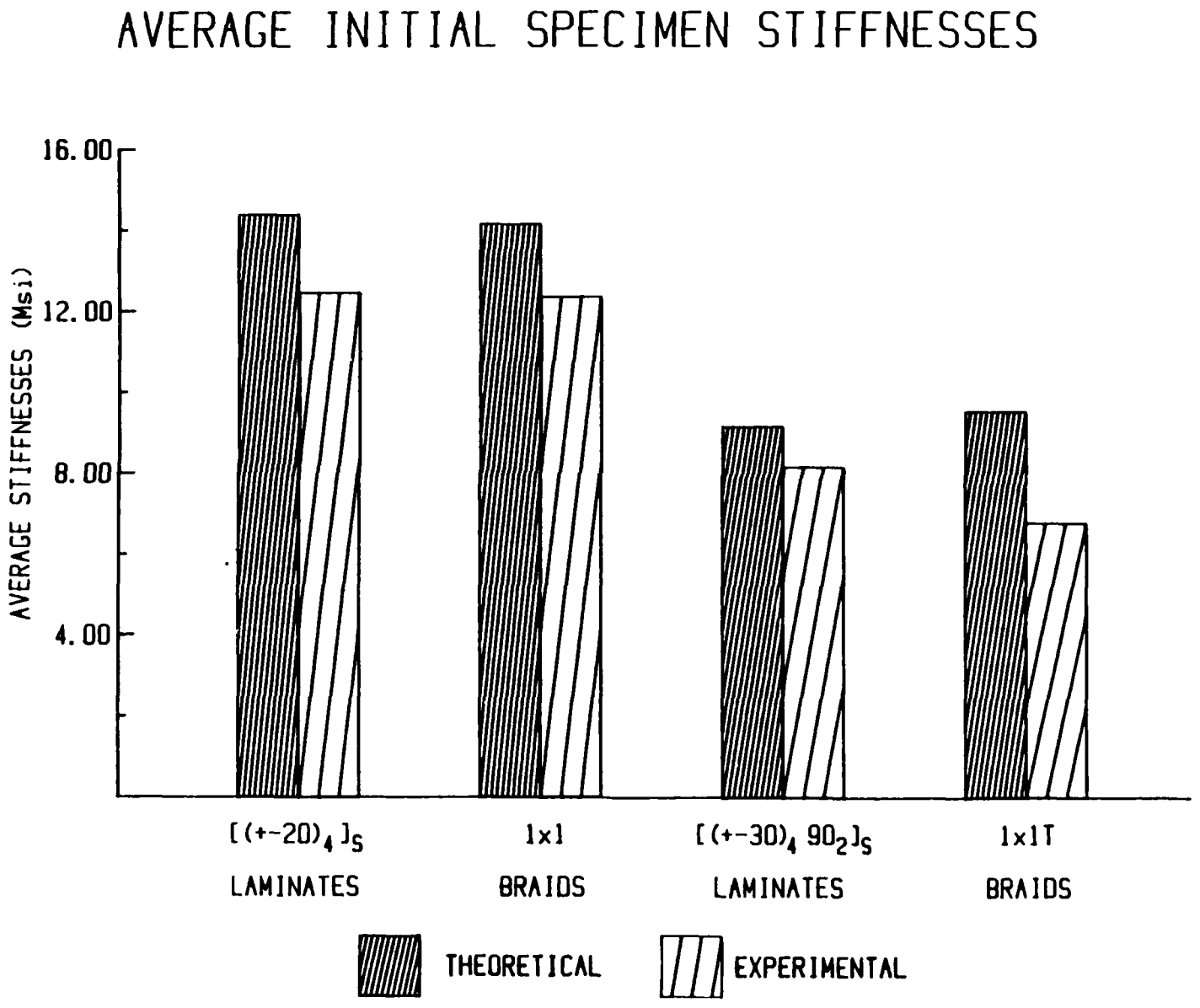

Fig. 13. Comparison of theoretical stiffness (E_{xx}) average experimental stiffness (E_{xx}).

INITIAL 1x1 BRAID STIFFNESSES

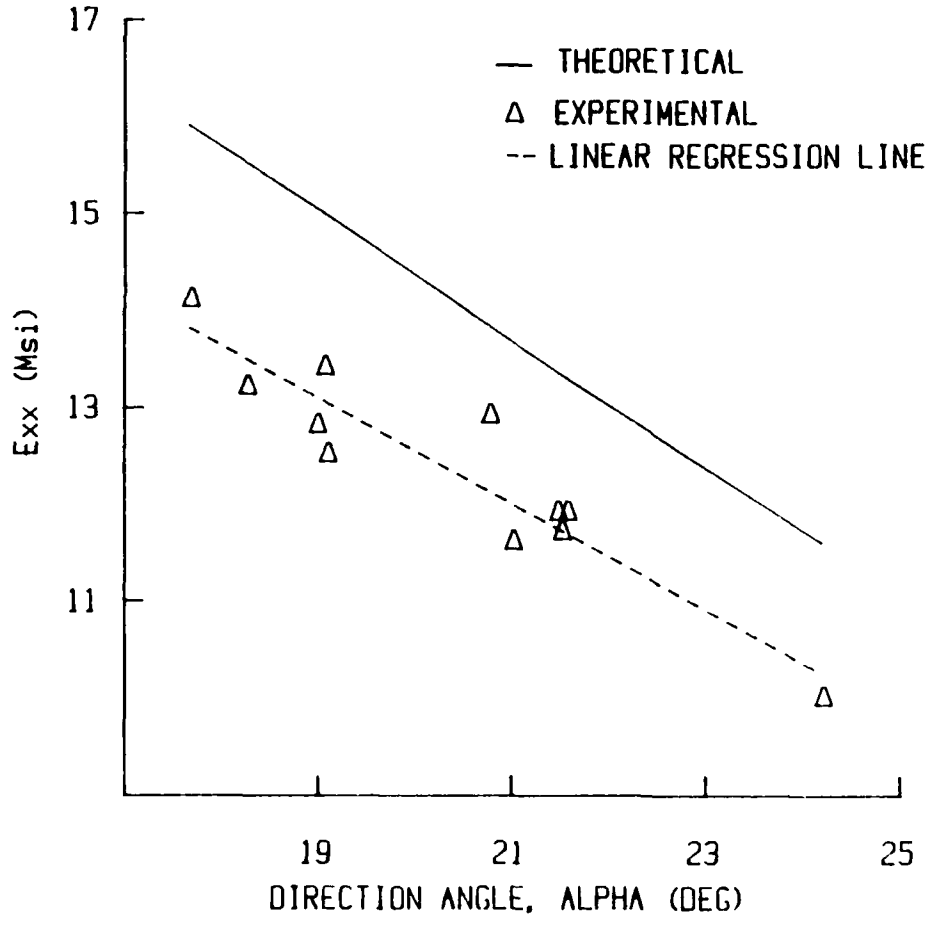

Fig. 14. Theoretical and experimental longitudinal stiffness for the 1 x 1 braided specimen set.

INITIAL 1x1T BRAID STIFFNESSES

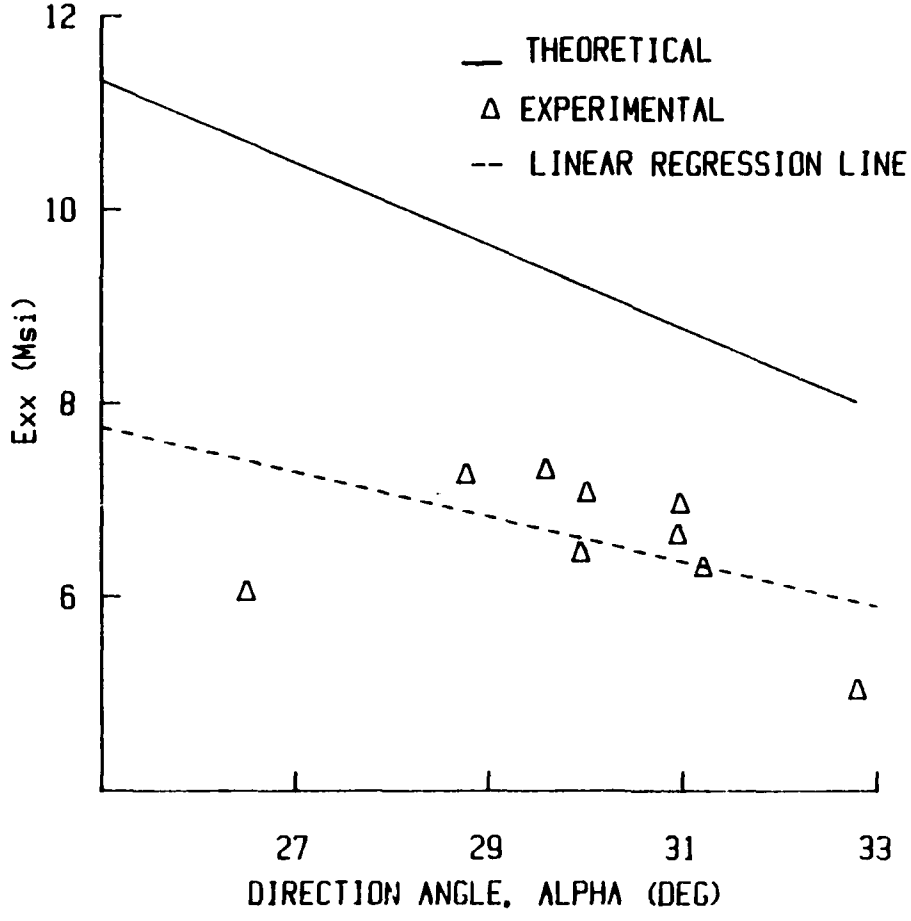

Fig. 15. Theoretical and experimental longitudinal stiffness for the 1 x 1T braided specimens.

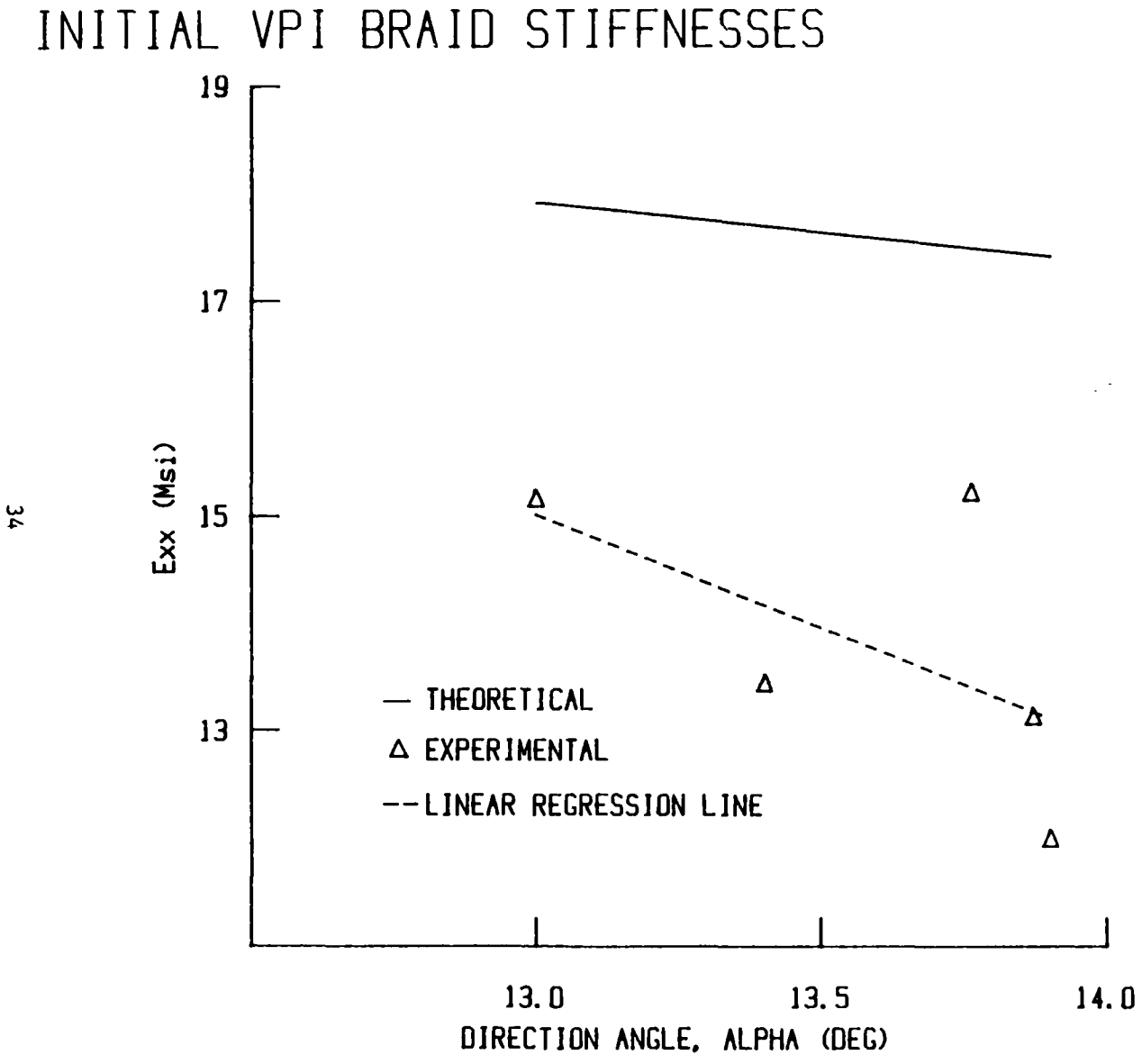

Fig. 16. Theoretical and experimental longitudinal stiffness for the 1 x 1 VPI braided specimens.

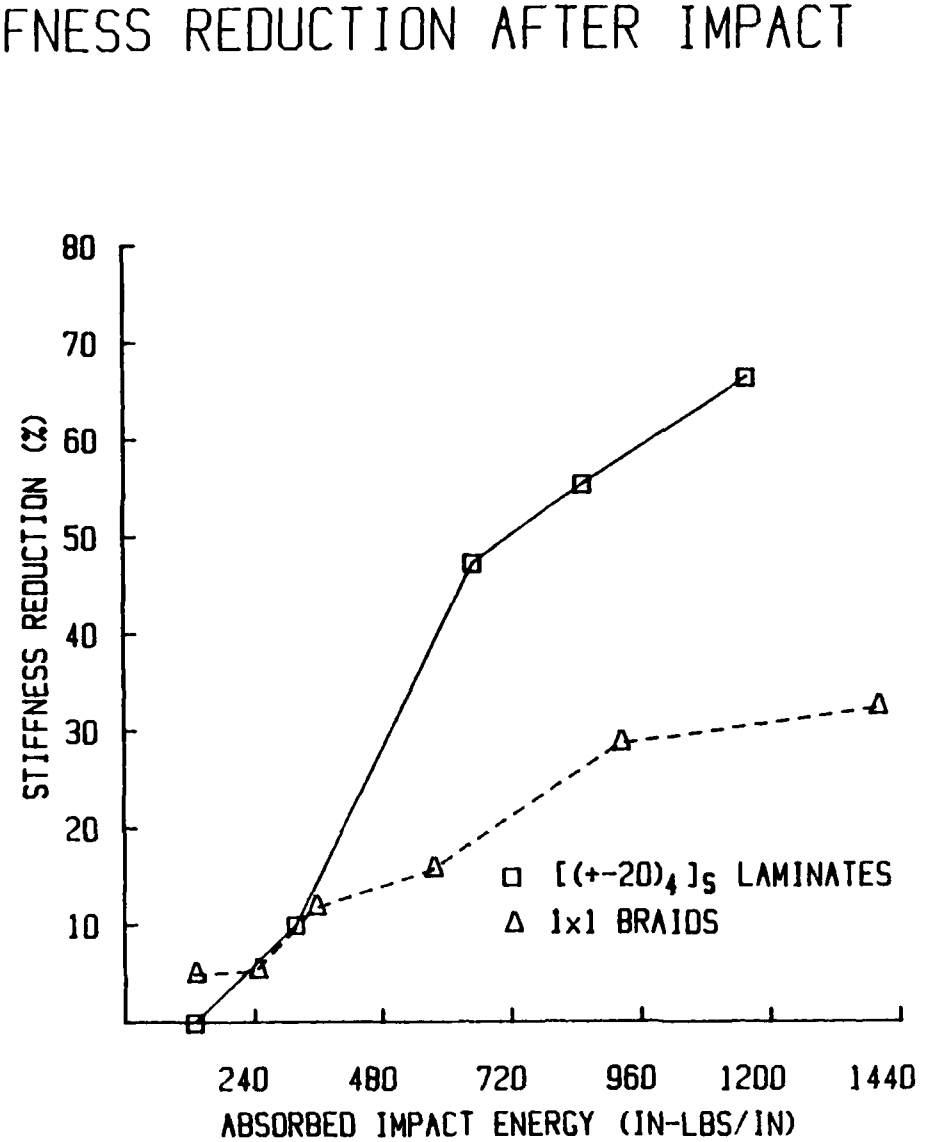

Fig. 17. Stiffness reduction after impact of 1 x 1 braided specimens.

STIFFNESS REDUCTION AFTER IMPACT

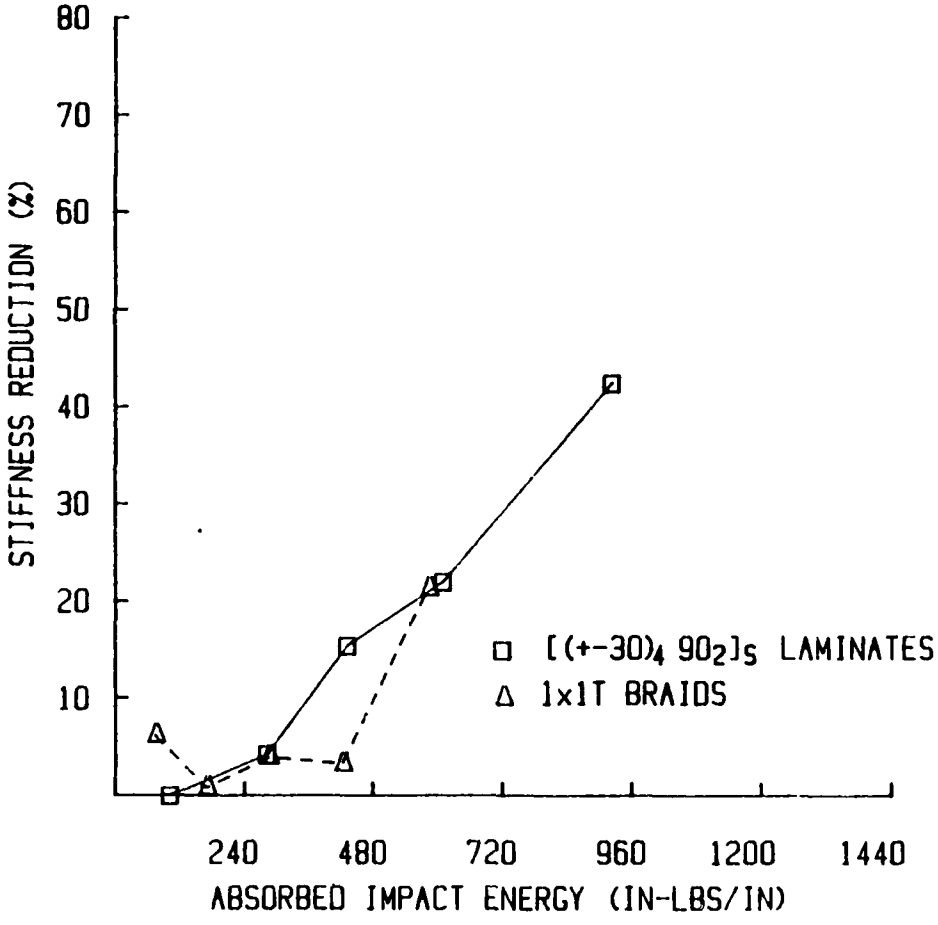

Fig. 18. Stiffness reduction after impact of 1 x 1T braided specimens.

reduction axis on the plots and Figs. 17 and 18 represents a ratio of stiffness after impact to stiffness prior to impact. The absorbed energy impact axis represents the total potential energy for the ball weight and height chosen, minus the rebound energy resulting from the ball rebound.

The significant result from this data is the stiffness retention capability of the 1x1 braid style compared to the ($\pm$20) angle ply laminates. The 1x1 braids retain 30% greater stiffness than the laminate at the higher impact energy levels.

The results from the dye-penetrant enhanced x-ray radiography studies are shown in Figs. 19 through 23. The x-rays in these figures are grouped in pairs by impact energy level for comparison of braided specimen and laminated specimen response. The damage patterns in the laminated specimens show distinct delamination and fiber-matrix splitting, as observed by many other investigators.

The damage patterns observed in the braided specimens evaluated in this program are made up of three modes of damage. The first type can be described as intertow cracking since it occurs between tows, and is evident on all 1x1 specimens to the outermost portion of the damage area. The second type of damage observed can be described as intratow cracking, and extends from the impact epicenter, but does not progress as far as intertow cracking. The third type of damage can be described as intertow delamination, and shows up as a dark halo in dye-penetrant enhanced x-rays, as delaminations appear in x-rays of laminates. All three damage modes can be observed for the 1x1 specimen types. A photograph containing examples of all three damage modes is shown in Fig. 24. For the 1x1T specimens, intertow cracking was present over the entire length and width of all impact specimens. These cracks were shown not

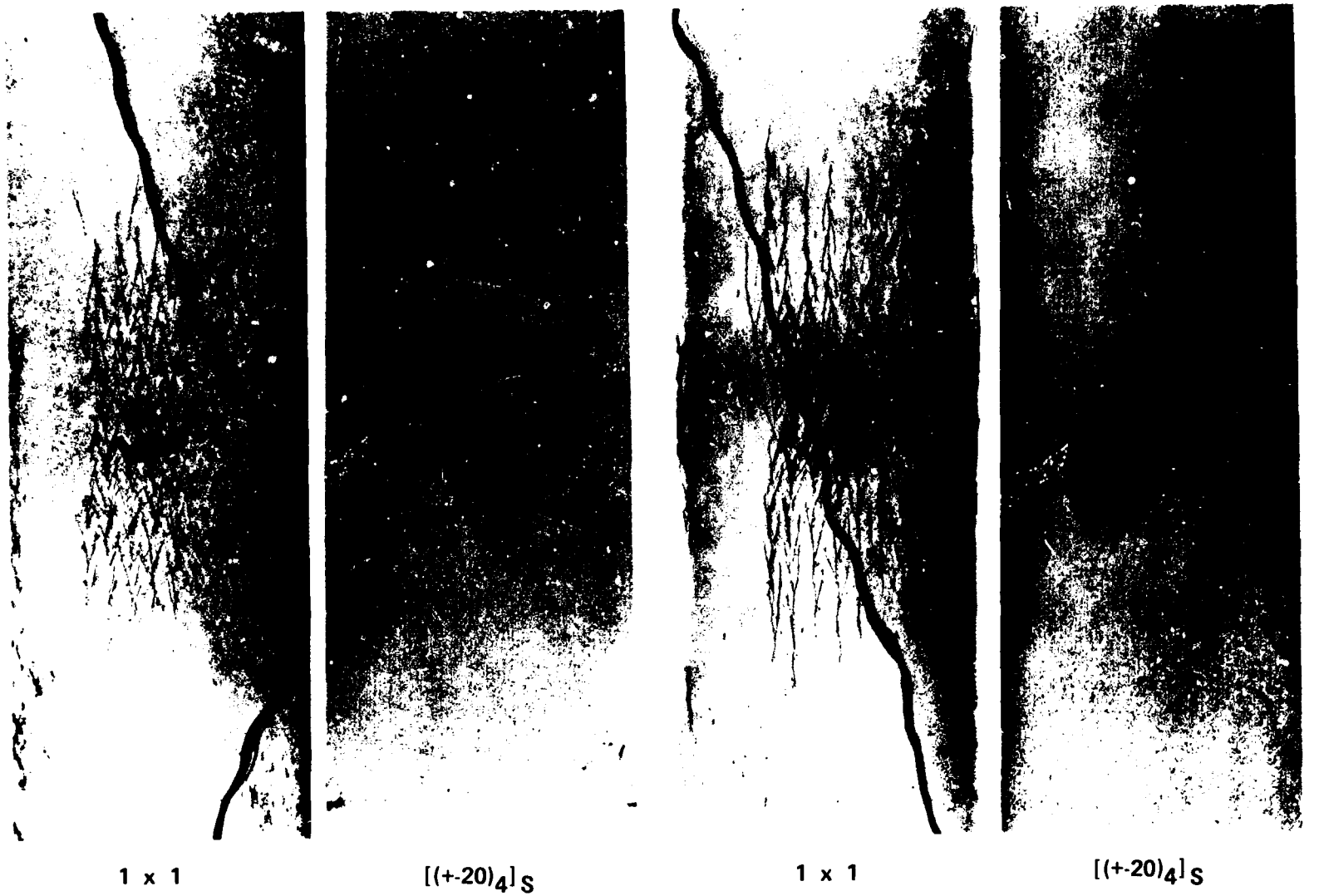

Fig. 19. Radiographs of 1 x 1 specimens and laminates impacted at 24 in-lbs and 48 in-lbs.

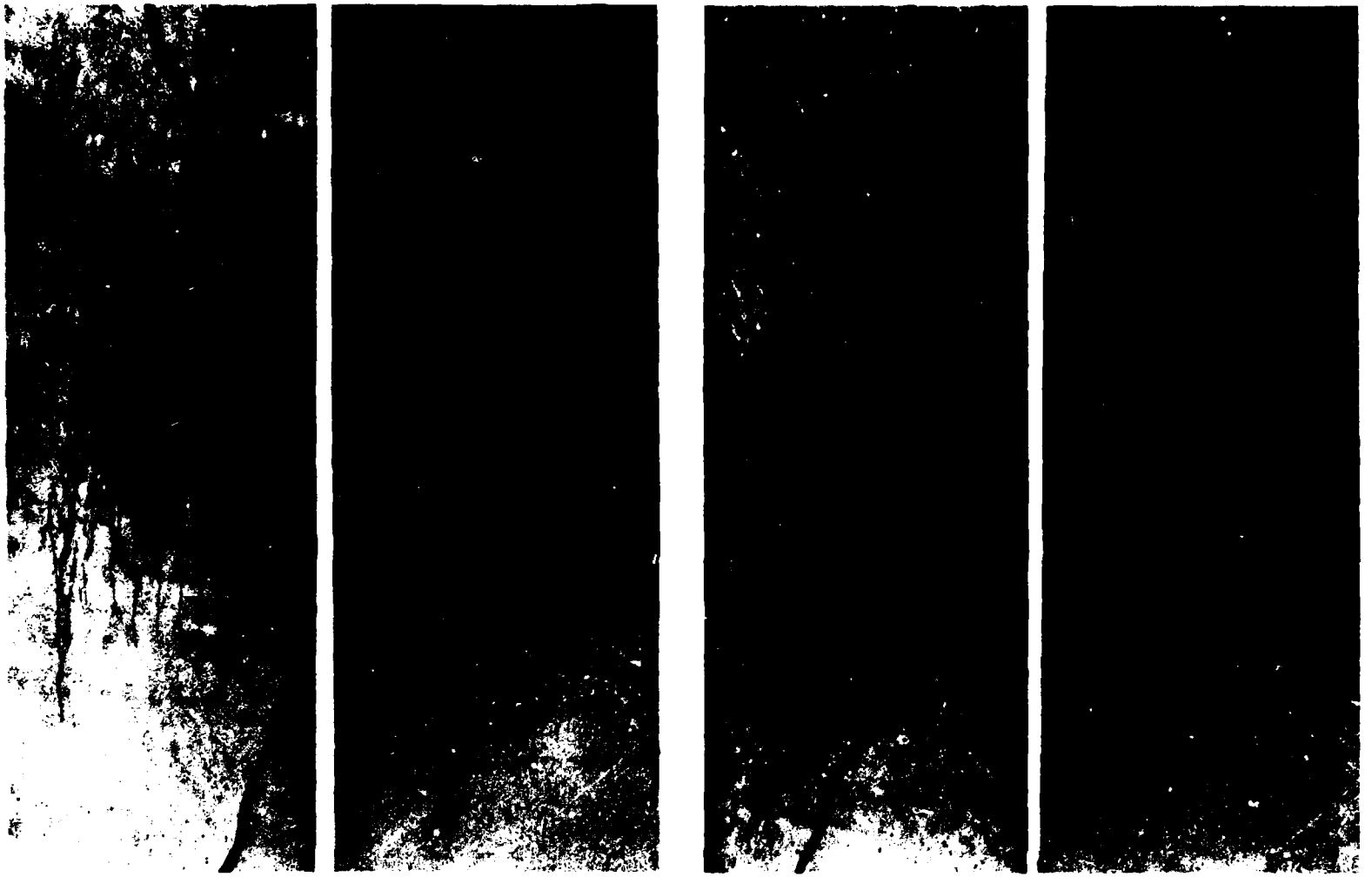

Fig. 20. Radiographs of 1 x 1 specimens and laminates impacted at 72 in-lbs and 96 in-lbs.

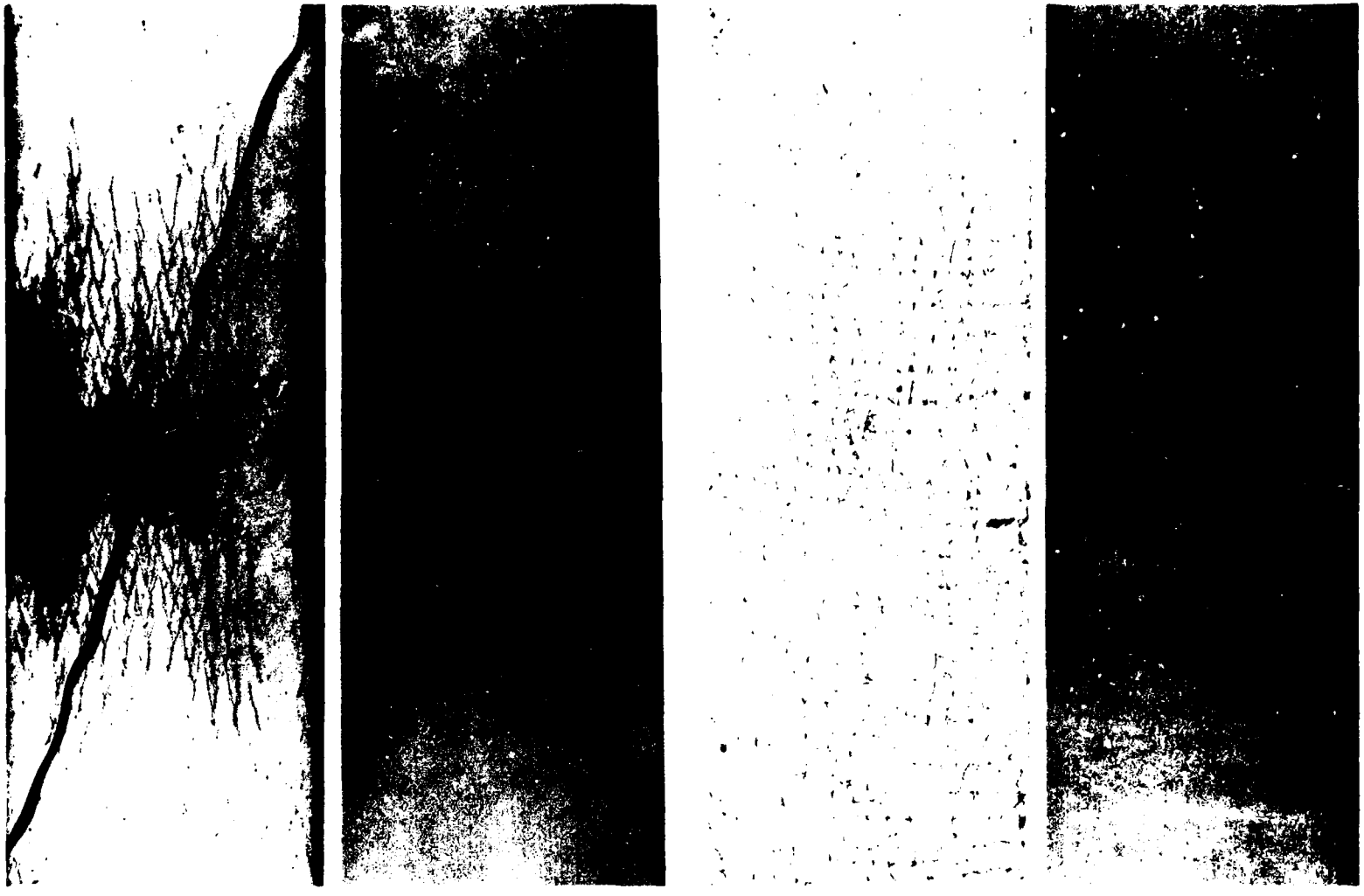

Fig. 21. Radiographs of a 1 x 1 specimen and laminate at 120 in-lbs and 1 x 1T specimen and laminate at 24 in-lbs.

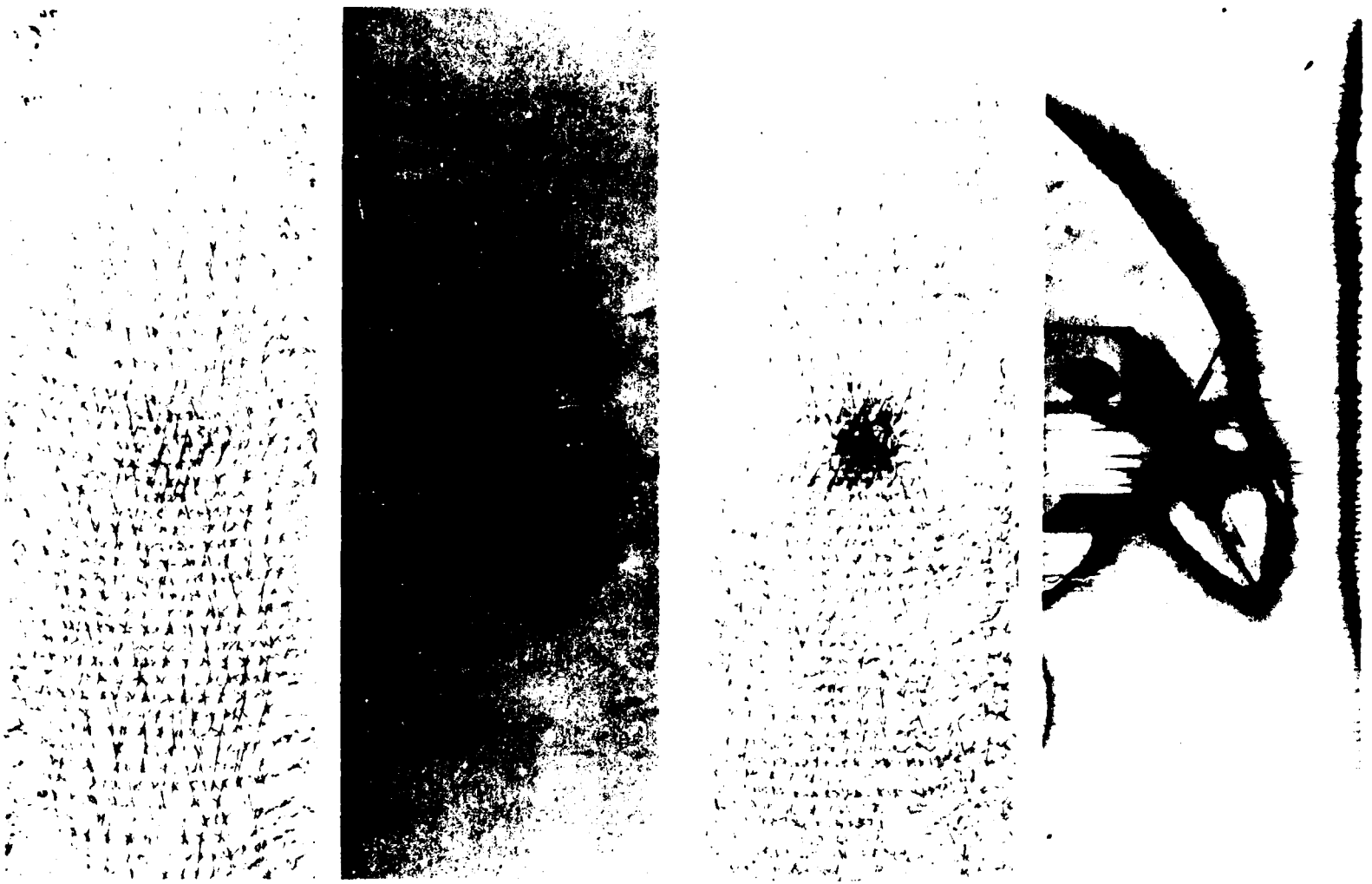

Fig. 22. Radiographs of 1 x 1T specimens and laminates impacted at 48 in-lbs and 72 in-lbs.

Fig. 23. Radiographs of 1 x 1T specimens and laminates impacted at 96 in-lbs and 120 in-lbs.

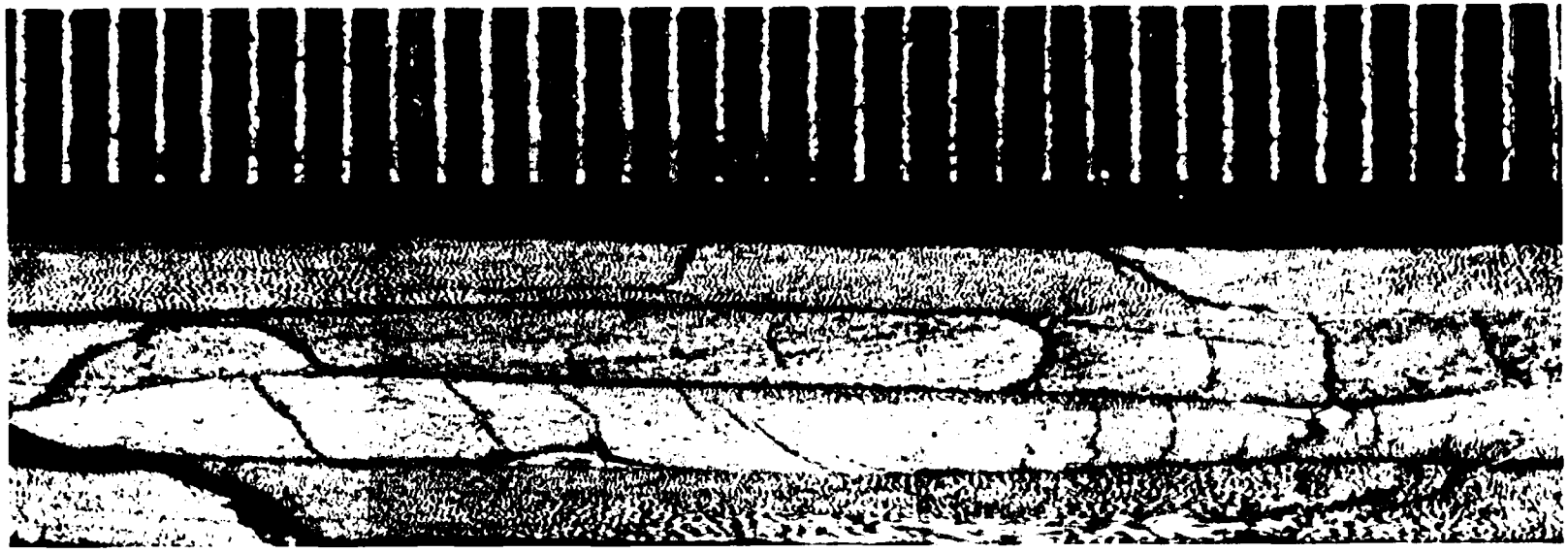

Fig. 24. Photomicrograph of a longitudinal section of specimen XD5 following impact.

to be associated with the impact event when an x-ray of an unimpacted 1x1T specimen exhibited the same crack patterns. This implies that the extensive intertow cracking in 1x1T specimens is due to thermomechanical cure stresses or the low level unaxial stress applied to each specimen during tension testing. The former cause is the most probable.

The extent of damage induced by the impact testing increased slightly with increasing impact energy levels, while the laminates showed a more evident increase in impact related damage with increasing energy levels.

Using the damage area and absorbed impact energy information from the drop-ball impact tests, values for E_{INT} (Eq. 3) were calculated using the impact damage model. The damage area was assumed to be rectangular for the 1x1 braids and circular for the 1x1T braids as indicated in the x-ray radiographs. The damage area used to calculate E_{INT} only included the area of intertow delamination due to the basic hypothesis of the model. The perimeter of the damage for both braids styles was assumed to be at the outer boundary of the dark intertow delamination area.

Table 7 lists the values for damage size and E_{INT} for each braid specimen evaluated.

Table 7. Damage size and intersection toughness.

Specimen	Absorbed Impact Energy (in-lb)	Damage Length (in.)	Damage Length (in.)	Damage Radius (in.)	Intersection Toughness E_{INT} (in-lb/in^2)
XD6	3.12	.438	.313	-	10.6
XD1	18.6	.750	.563	-	2.74
XD3	24.8	.875	.688	-	2.13
XD4	67.8	.750	.625	-	9.44
XD5	96.0	.875	.750	-	7.96
XD5T	8.34	-	-	.219	6.56
XD6T	19.2	-	-	.281	7.42
XD7T	35.4	-	-	.281	11.62
XD8T	52.3	-	-	.418	4.19
XD9T	72.1	-	-	.500	2.78

The values for E_{INT} in Table 7 were calculated based on a Mode II strain energy release rate of 3.0 in-lb/in^2 for the T300/5208 graphite epoxy material system. This value of G_{II} was based on work done by Bostaph and Elber.[12]

For each value of E_{INT} generated by a single drop ball impact test, a theoretical plot of impact damage versus impact energy can be generated. These theoretical plots, one for each impact test, as shown in Figs. 25 through 28. In these figures, the solid triangles represent the data points from the drop balll impact tests on the ten braided specimens. From each of these data points a value of E_{INT} was calculated and used to generate a set of theoretical data relating impact damage to impact energy. The theoretical data are shown on one line in each of figures 25 through 28. Each set of data was curve fit using a cubic spline curve futting routine and for clarity only this line is shown for four of the five plots on each figure.

For the best correlation between theoretical and experimental results, E_{INT} should be the same when calculated for any impact energy level, and all five plots in figures 25 through 28 should lie one on top of the other. Therefore, the results of the impact damage model show greater accuracy for the 1x1T braids than for the 1x1 braids. The results for the 1x1 braids are encouraging however and an average representation for the correlation between impact damage and impact energy is represented by the curve generated by specimen XD5.

RECOMMENDATIONS

As a result of this theoretical and experimental investigation, it is recommended that the following topics be more fully explored. The exact cause of the extensive intertow cracking in the 1x1T braids should be

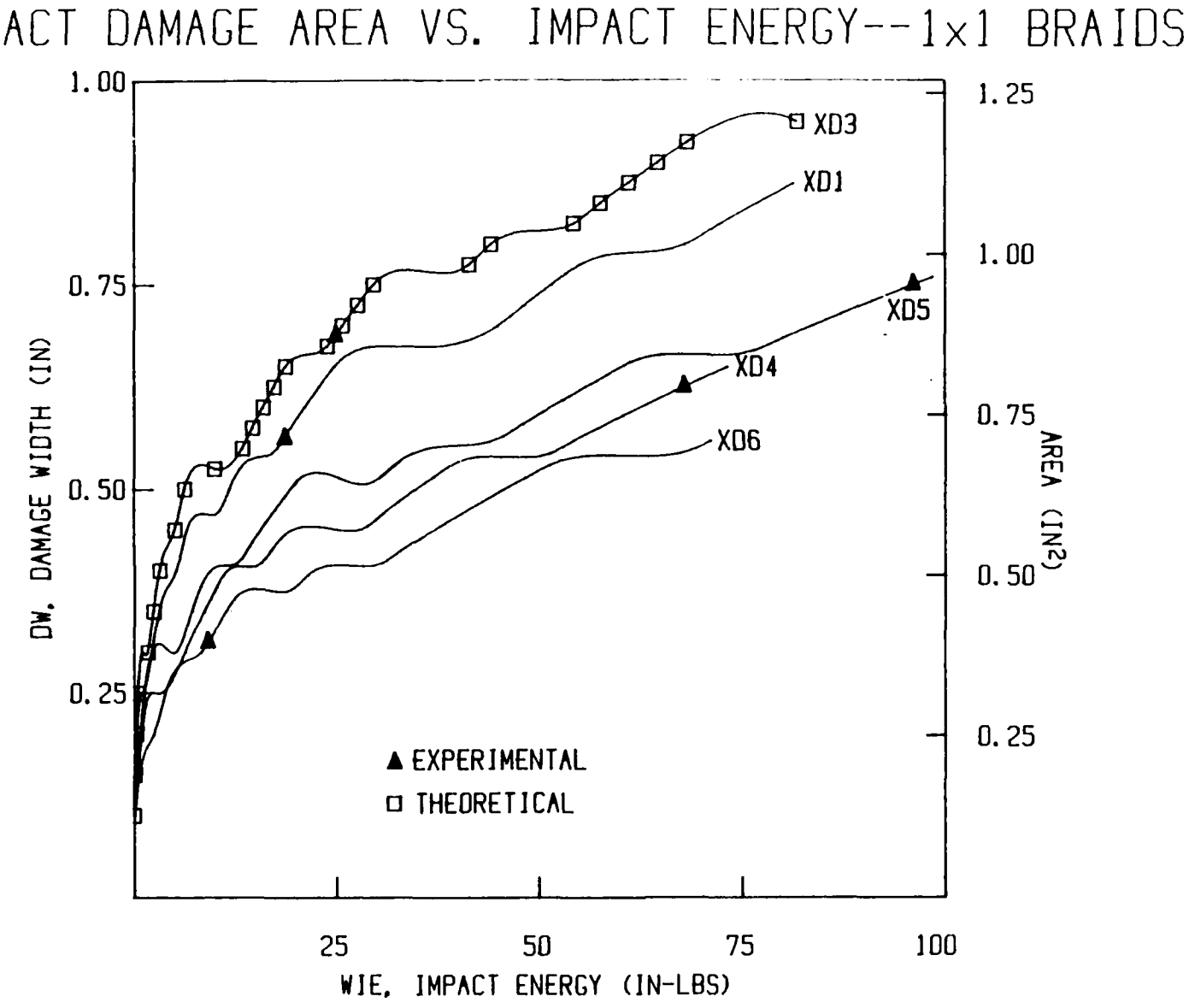

Fig. 25. Graph of impact damage vs. impact energy for 1 x 1 braids from 0 to 100 in-lbs.

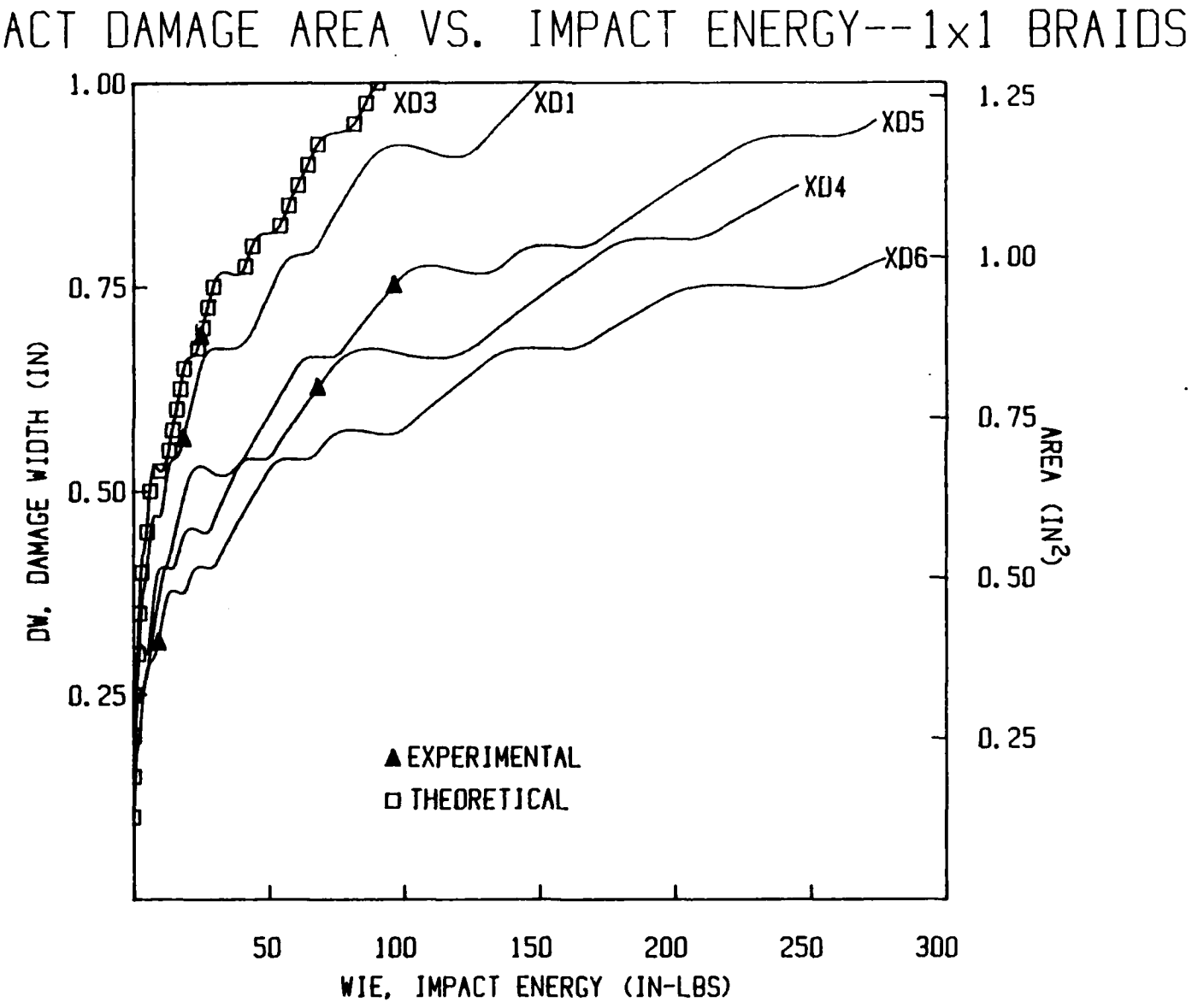

Fig. 26. Graph of impact damage vs. impact energy for 1 x 1 braids from 0 to 300 in-lbs.

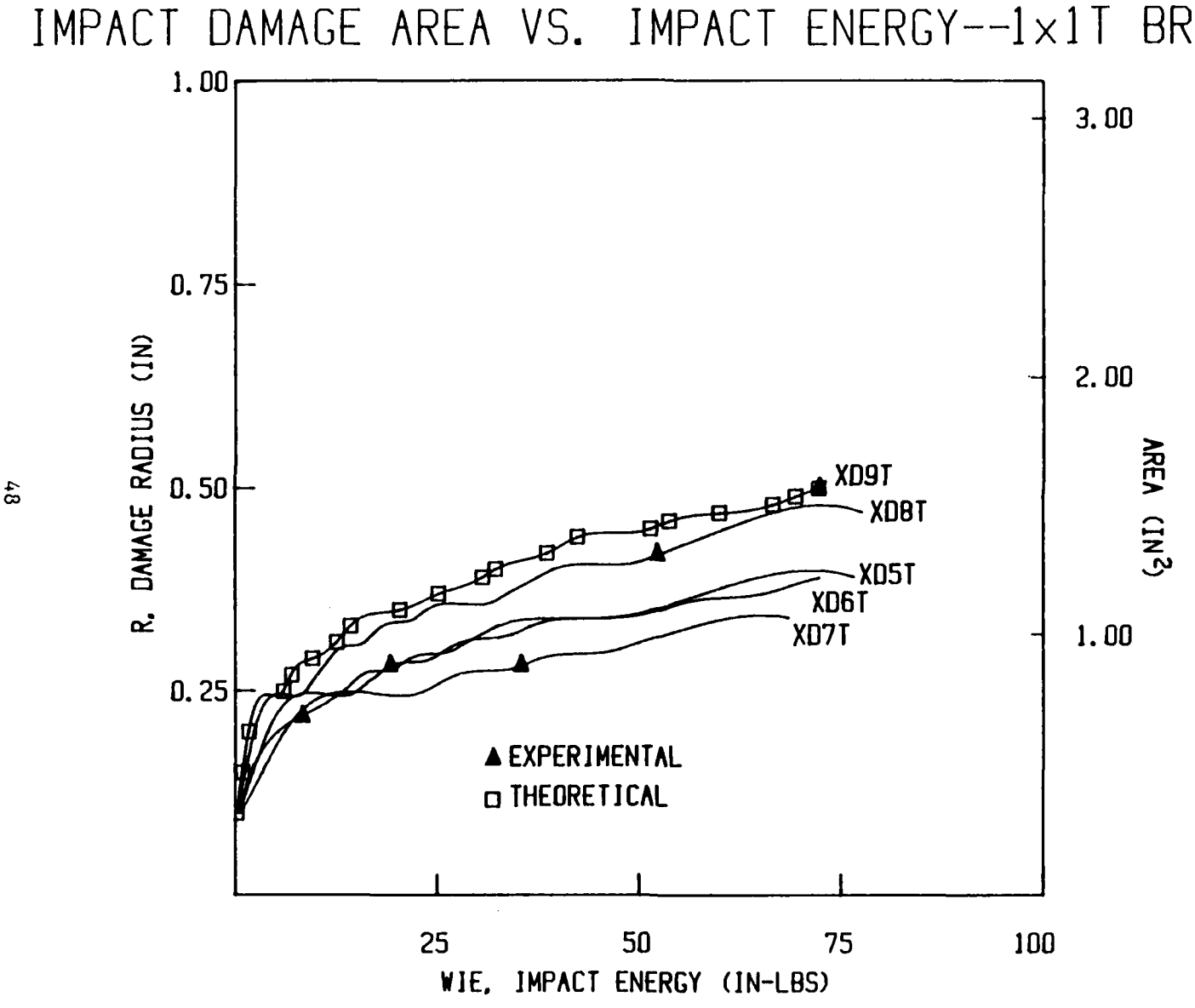

Fig. 27. Graph of impact damage vs. impact energy for 1 x 1T braids from 0 to 100 in-lbs.

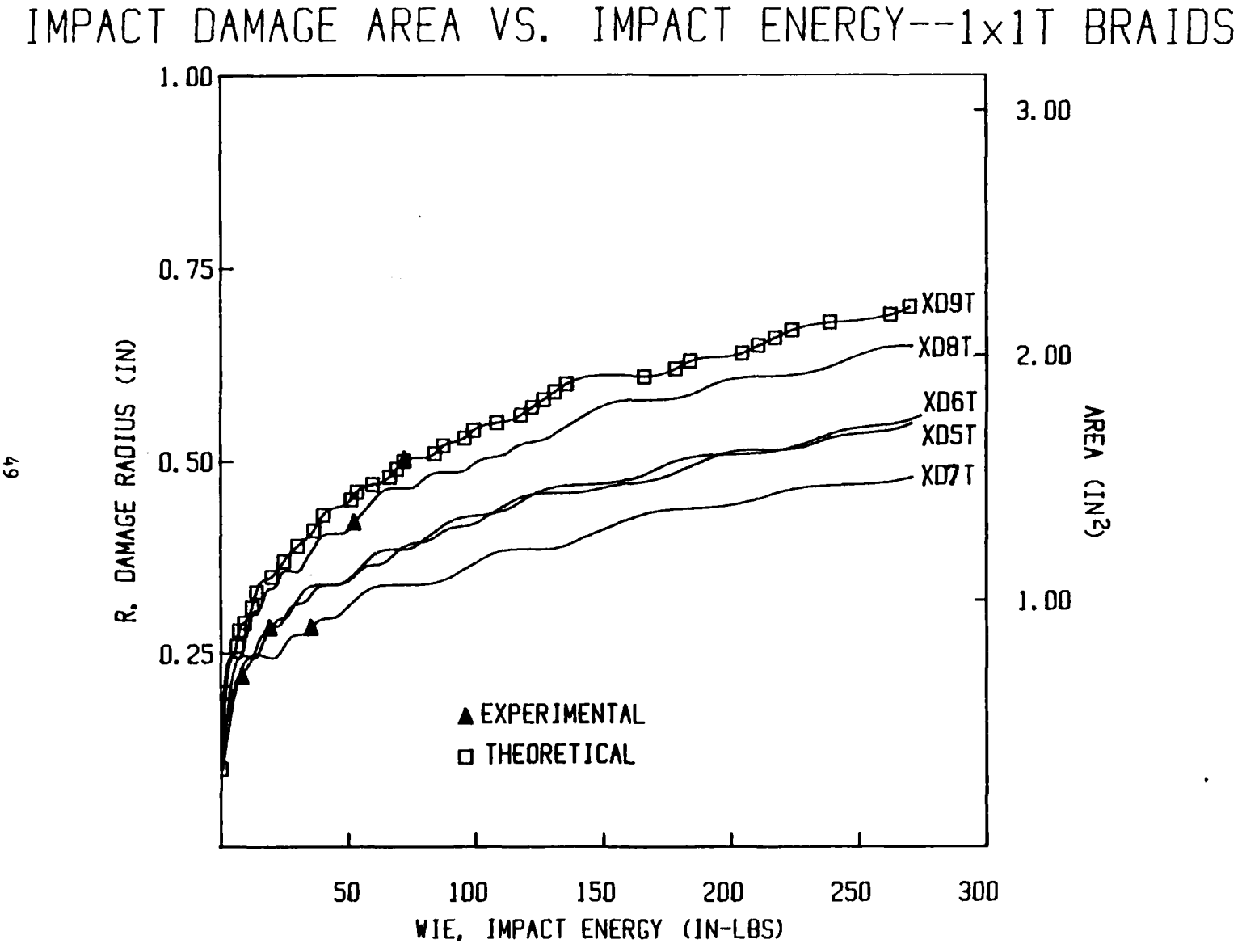

Fig. 28. Graph of impact damage vs. impact energy for 1 x 1T braids from 0 to 300 in-lbs.

determined. Work should then be conducted to eliminate these cracks and efforts should also be made to eliminate the resin rich and high void areas which occur in the transverse filled specimens.

A comparison of the theoretical stiffness model with experimental transverse stiffness experiments is also warranted. The proposed model has has been shown to be accurate for longitudinal stiffness, and should likewise be accurate for transverse data.

Finally, the impact damage model should be compared with experimental data from specimens greater than two inches wide to eliminate any edge effects influencing impact results.

CONCLUSIONS

The fiber geometry described in this report relates the fundamental braid parameters, which describe the textile process used to manufacture braided composites, to the three-dimensional fiber geometry of the finished composite element. The results from this model provided an accurate representation of the fiber geometry neglecting tow thickness and tow undulation at intersection points.

The stiffness model developed here provides a means to determine changes in the principal geometric stiffness parameters (E_{xx}, E_{yy}, E_{zz}) resulting from changes in braiding parameters and fiber geometry. Minor differences in fiber geometry and stiffness between braids of the same construction were accounted for by both the fiber geometry and stiffness models. The effect of unidirectional fill fibers were also accounted for accurately by the stiffness model.

The semi-empirical impact damage model provides a method for relating the impact energy imparted to a braided composite to the resulting impact

damage. This model also provides an estimate for the contribution of fiber intersection toughness to the toughness of a graphite/epoxy braided panel. The results of the impact damage model show excellent consistency for a 1x1T braided construction, and fair-to-good consistency for a 1x1 braided construction.

Finally, the development of impact damage within a braided composite material was documented and shown to be substantially different than for laminates subjected to the same conditions. The preference for cracking (intertow and intratow) over intertow delamination was evident.

ACKNOWLEDGMENT

The authors would like to thank Dr. Dave Moran and Mr. Joe Crisci for their financial support and encouragement during this research program.

APPENDIX A

DATA SUPPORTING TIME FIBER GEOMETRY, STIFFNESS, AND IMPACT DAMAGE MODELS

```
10  PRINT TAB(37);"CIRCULAR IMPACT ENERGY, CIRIMEN "
20 INPUT "SPEC. NUM.";SPECN$
30 PRINT "NC"
40 INPUT NC
50 PRINT "RMY"
60 INPUT RMY
70 PRINT "PPL"
80 INPUT PPL
90 PRINT "GII"
100 INPUT GII
110 PRINT "WIDTH"
120 INPUT W
130 PRINT "R"
140 INPUT R
150 PRINT "EINT"
160 INPUT EINT
170 LPRINT "SPEC NUM"; SPECN$
180 LPRINT "NC=";NC
190 LPRINT "RMY=";RMY
200 LPRINT "PPL=";PPL
210 LPRINT "GII=";GII
220 LPRINT "WIDTH=";W
230 LPRINT "R=";R
240 LPRINT "EINT=";EINT
250 PRINT "R"
260 INPUT R
270 NSUM=0
280 Y=2*W/(NC-RMY-1)
290 D=Y/2
300 IF D*D)R*R THEN IF D(0 THEN 340
310 IF D)R THEN 360
320 C=2*SQR(R^2-D^2)
330 NSUM=INT(C*PPL+1)+NSUM
340 D=D+Y
350 GOTO 300
360 N=2*NSUM
370 DA=3.141593*R*R
380 WIE=DA*(GII+N*EINT)
390 EH=(WIE-DA*GII)/(DA*N)
400 LPRINT "R=";R;"      WIE=";WIE
410 PRINT "ANY MORE VALUES, 1=YES, 0=NO"
420 INPUT V
430 IF V=0 THEN END
440 IF V=1 GOTO 250
```

Fig. A.1. Listing of computer program used to calculate circular impact damage area.

```
10  PRINT TAB(37);"IMPACT ENERGY"
20 INPUT "SPEC. NUM.";SPECN$
30 PRINT TAB(37);"IMPACT ENARGY"
40 PRINT "NC"
50 INPUT NC
60 PRINT "RMY"
70 INPUT RMY
80 PRINT "PPL"
90 INPUT PPL
100 PRINT "GII"
110 INPUT GII
120 PRINT "WIDTH"
130 INPUT W
140 PRINT "DW"
150 INPUT DW
160 PRINT "DL"
170 INPUT DL
180 PRINT "EINT"
190 INPUT EINT
200 DR=DL/DW
210 LPRINT "SPEC MUM"; SPECN$
220 LPRINT "NC=";NC
230 LPRINT "RMY=";RMY
240 LPRINT "PPL=";PPL
250 LPRINT "GII=";GII
260 LPRINT "WIDTH=";W
270 LPRINT "DW=";DW
280 LPRINT "DL=";DL
290 LPRINT "DR=";DR
300 LPRINT "EINT=";EINT
310 PRINT "DW"
320 INPUT DW
330 WI=DR*DW^2*GII
340 WE=DR*DW^2*EINT*INT(DR*DW*PPL+1)*INT(DW*(NC-RMY-1)/(2*W)+1)
350 WIE=WI+WE
360 LPRINT "DW=";DW;"      WIE=";WIE
370 PRINT "ANY MORE VALUES, 1=YES, 0=NO"
380 INPUT V
390 IF V=0 THEN END
400 IF V=1 GOTO 310
```

Fig. A.2. Listing of computer program used to calculate rectangular impact damage area.

Table A.1 Braid parameters and direction angles for 1x1 braided specimens.

Input Braid Parameters

NR = 5
NC = 32
RMY = 1
CMZ = 1

Specimen	Thickness (in.)	Width (in.)	PPL	Theta XY (°)	Theta XZ (°)	Alpha (°)	Beta (°)	Gamma (°)
XD1	0.0760	1.9685	3.33	17.73	7.21	18.98	72.40	83.13
XD2	0.0743	2.0007	3.63	19.51	7.68	20.76	70.65	82.76
XD3	0.0700	2.0030	3.07	16.70	6.13	17.67	73.39	84.12
XD4	0.0737	2.0058	3.76	20.20	7.89	21.46	69.98	82.59
XD5	0.0678	2.0035	3.34	18.08	6.46	19.06	72.03	83.86
XD6	0.0710	2.0035	3.80	20.37	7.68	21.56	69.79	82.79
XD7	0.0765	2.0140	4.26	22.71	9.25	24.19	67.56	81.45
XD8	0.0728	2.0070	3.16	17.19	6.56	18.27	72.92	83.73
XD9	0.0745	2.0070	3.76	20.21	7.97	21.50	69.97	82.51
XD10	0.0737	2.0187	3.65	19.77	7.66	21.00	70.39	82.79
XD11	0.0723	2.0050	2.88	15.73	5.94	16.72	74.35	84.28
XD12	0.0737	2.0053	3.31	17.94	6.95	19.09	72.18	83.38

Table A.2 Braid parameters and direction angles for 1x1T braided specimens.

Input Braid Parameters

NR = 5
NC = 32
RMY = 1
CMZ = 1

Specimen	Thickness (in.)	Width (in.)	PPL	Theta XY (°)	Theta XZ (°)	Alpha (°)	Beta (°)	Gamma (°)
XD0T	0.1270	2.0117	5.51	28.40	19.28	32.78	62.96	72.89
XD1T	0.1000	2.0023	3.45	18.62	9.79	20.73	71.63	80.72
XD2T	0.1080	2.0040	5.08	26.41	15.34	29.57	64.41	76.20
XD3T	0.1115	2.0080	5.12	26.63	15.93	29.99	64.25	75.69
XD4T	0.1120	2.0037	5.32	27.47	16.59	30.93	63.51	75.19
XD5T	0.1130	2.0043	5.31	27.44	16.70	30.95	63.56	75.09
XD6T	0.1128	2.0050	4.86	25.42	15.33	28.75	65.37	76.10
XD7T	0.1238	2.0057	5.23	27.10	17.94	31.20	64.04	73.92
XD8T	0.1238	2.0080	4.30	22.84	14.90	26.48	67.85	76.22
XD9T	0.1238	2.0020	4.98	25.94	17.13	29.93	65.07	74.51

Table A.3 Braid parameters and direction angles for 1x1 VPI braided specimens.

Input Braid Parameters

NR = 7
NC = 16
RMY = 1
CMZ = 1

Specimen	Thickness (in.)	Width (in.)	PPL	Theta XY (°)	Theta XZ (°)	Alpha (°)	Beta (°)	Gamma (°)
41	0.1210	1.0030	2.01	12.63	4.63	13.40	77.41	85.48
42	0.1230	0.9970	2.09	13.04	4.90	13.87	77.01	85.23
43	0.1240	0.9980	2.07	12.93	4.89	13.76	77.12	85.23
44	0.1250	0.9990	2.11	13.18	5.02	14.05	76.87	85.11
45	0.1240	1.0020	1.96	12.31	4.63	13.10	77.73	85.47
46	0.1230	1.0000	1.95	12.23	4.57	13.00	77.81	85.53
47	0.1230	1.0000	1.93	12.10	4.52	12.88	77.93	85.58
48	0.1210	0.9970	1.95	12.19	4.50	12.95	77.85	85.60
49	0.1200	0.9980	2.10	13.11	4.80	13.90	76.94	85.32
50	0.1170	1.0060	1.92	12.11	4.28	12.81	77.92	85.81

Table A.4 Comparison of theoretical and experimental stiffness of 1x1 braided specimens.

Specimen	Exx (10^6 lbf/in^2)	
	Theoretical	Experimental
XD1	15.1	12.8
XD2	13.9	12.9
XD3	15.9	14.1
XD4	13.4	11.9
XD5	15.0	13.4
XD6	13.3	11.9
XD7	11.6	10.0
XD8	15.5	13.2
XD9	13.4	11.7
XD10	13.7	11.6
XD12	15.0	12.5
Avg.	14.2	12.4

Table A.5 Comparison of theoretical and experimental stiffness of 1x1T braided specimens.

Specimen	Exx (10^6 lbf/in^2)	
	Theoretical	Experimental
XD0T	8.0	5.02
XD1T	13.1	8.99
XD2T	9.36	7.29
XD3T	9.18	7.05
XD4T	8.77	6.62
XD5T	8.77	6.94
XD6T	9.71	7.24
XD7T	8.66	6.28
XD8T	10.7	6.03
XD9T	9.20	6.43
Avg.	9.55	6.79

Table A.6 Comparison of theoretical and experimental stiffness of 1x1 VPI braided specimens.

Specimen	Exx (10^6 lbf/in^2)	
	Theoretical	Experimental
41	17.7	13.42
42	17.4	13.11
43	17.5	15.20
46	17.9	15.14
49	17.4	11.98
Avg.	17.54	13.77

REFERENCES

1. Macander, A.B., Crane, R.M., Camponeschi, E.T., "Fabrication and Mechanical Properties of X-D Braided Composite Panels," presented at the ASTM Seventh Symposium on Composite Materials; Testing and Design, April 1984.
2. Gause, L.W. and Alper, J.M., "Mechanical Properties of Magnaweave Composites," NADC Report No. NADC-84030-60, December 1983
3. Macander, A.B., Crane, R.M., Camponeschi, E.T., Jr., "The Fabrication, Processing and Characterization of Multidimensinally Braided Graphite/Epoxy Composite Materials", DTNSRDC/SME-84-66, July 1984.
4. Brunneschweiler, "Braids and Braiding," Textile Institute Journal, Vol. 44, No. 9, Sept 1953, pp. 140-167.
5. Wilkins, D.J., Eisenmann, J.R., Camin, R.A., Margolis, W.S., and Bensor, R.A., "Characterizing Delamination Growth in Graphite-Epoxy," Damage in Composite Materials, ASTM STP 775, ASTM, 1982 pp. 168-183.
6. O'Brien, T.K. "Characterization of Delamination Onset and Growth in a Composite Laminate," Damage in Composite Materials STP 775, ASTM 1982, pp. 140-167.
7. Russell, A.J. and Street, K.N., "Moisture and Temperature Effects on the Mixed-Made Delamination Fracture of Unidirectional Graphite/Epoxy," Delamination and Debonding of Materials, ASTM STP 876, ASTM, 1985, pp. 349-370.
8. Masters, J.E., "Characterization of Impact Damage Development in Graphite/Epoxy Laminates," Presented at ASTM Symposium on Fractography of Modern Engineering Materials, Nov. 1985.
9. Stinchcomb, W., Simonds, R.A., and Jones, R.M., Virginia Tech Report CCMS-84-18, VPI & SU Blacksburg, VA June 1985.
10. Crane, R.M. and Macander, A.B., "Invention Disclosure for Resin Impregnation and Processing Techniques for Rigidizing Net-Shaped Fibrous Skeletal Composite Preforms," Navy Case #67962, filed Oct 1982.

11. Rummel, W.D., Tedrow, T., and Brinkerhoff, M.D., "Enhanced X-Ray Stereoscopic NDE of Composite Materials," Final Report AFWAL-TR-80-3053, June 1980.

12. Bostaph, G.M. and Elber, W., "A Fracture Mechanics Analysis for Delamination Growth During Impact on Composite Plates," 1983 Advances on Aerospace Structures, Materials and Dynamics; Proceedings of ASME Annual Meeting, pp. 133-138.

INITIAL DISTRIBUTION

Copies	
1	NRL Code 6383 (Wolock)
1	NADC Code 6043 (Gauss)
1	NSWC Code R31 (Weller)
3	NAVSEA 1 SEA 05M3 (Lovell) 1 SEA 05M3 (Pinto) 1 SEA 05R4 (Freund)
6	DTIC

CENTER DISTRIBUTION

Copies	Code	Name
1	012.3	(Moran)
1	012	(Caplan)
1	17	(Krenzke)
1	172	(Rockwell)
1	1720	(Phyillaier)
1	1720.6	(Macander)
1	1730.2	(Critchfield)
1	2722	(Ward)
1	2723	(Wilhelmi)
1	28	(Wacker)
1	2801	(Crisci)
1	2803	(Cavallaro)
1	284	(Fischer)
12	2844	(Camponeschi)
1	522.2	(Unclass Lib)
1	5231	(Office Services)

DTNSRDC ISSUES THREE TYPES OF REPORTS:

1. **DTNSRDC reports, a formal series,** contain information of permanent technical value. They carry a consecutive numerical identification regardless of their classification or the originating department.

2. **Departmental reports, a semiformal series,** contain information of a preliminary, temporary, or proprietary nature or of limited interest or significance. They carry a departmental alphanumerical identification.

3. **Technical memoranda, an informal series,** contain technical documentation of limited use and interest. They are primarily working papers intended for internal use. They carry an identifying number which indicates their type and the numerical code of the originating department. Any distribution outside DTNSRDC must be approved by the head of the originating department on a case-by-case basis.

END

11-86

DTIC